POLITECNICO DI TORINO

Master's Degree in MECHATRONIC ENGINEERING

Politecnico di Torino

Master's Degree Thesis

Enhancing Tracking Algorithm Performance in a 2D Laser Cutting Machine through Z-Axis Modelling and Validation

Supervisor

Prof. Alessandro Rizzo

Company Supervisor

David Tulli

Candidate

Domenico Manzari

July 2024

Abstract

This work arises from the need to solve the problem of tracking the signal from a capacitive sensor and was promoted by Prima Industrie, a leader in the production of laser cutting machines for sheet metal.

The quality of laser cutting significantly depends on the distance between the cutting head and the sheet. An algorithm controls this distance in real time by tracking the capacitive sensor signal to ensure the correct standoff.

To compensate for system delays and optimize cutting performance, the system, particularly the Z-axis, was modelled using a data-driven approach based on experimental tests, exciting the system with white noise added to the different control loops. Data processing and analysis led to the development of a model using MATLAB® System Identification Toolbox.

Finding and using new components to integrate into the machine to improve its performance required the creation of a physics-based model, taking a first-principles approach through the Bond Graph Approach. Both. Subsequently, the models were implemented in MATLAB and Simulink. The activity concluded with validation and comparison of the two modelling approaches against a reference signal. Suggestions for future developments were provided to improve the models and consequently the analysis of signal tracking and cutting quality.

INDEX

List of Figures

List of Tables

1 INTRODUCTION

1.1 STUDY OF ARTS

The present work was performed in collaboration with the company Prima Power, a member of the Prima Industrie group, manufacturer of machinery for cutting sheet metal by laser.

The activity stems from the company's need to investigate the characterisation of the performance of what takes place in the cutting process, particularly regarding the distance between the cutting head and the sheet metal.

The machinery to be used for 2D laser cutting of sheet metal recorded some undesirable malfunctions related to the cutting process. In particular, the malfunctions reported are related to phenomena called tip-touch, i.e. when the tool mounted at the end of the cutting head touches the sheet metal. The distance between the tip (cutting head) and the sheet metal is managed by a tracking algorithm, integrated in the PLC, which guarantees that the distance known as StandOff is constant even after variations. Increased cutting power and increased performance in terms of jerk, Jerk is the time derivative of acceleration, and thus is associated with rapidly changing actuator forces. Excessive jerk leads to premature wear on the actuators, induces resonant vibrations in the robot's structure, and is difficult for a controller to track accurately.[1]

The work started with an analysis of the evaluation of delays in the system, which adversely affect the tracking performance of the signal. Two signals were used for this evaluation, the signal read by the capacitance sensor placed on the cutting head, and the moment when the motor receives the command.

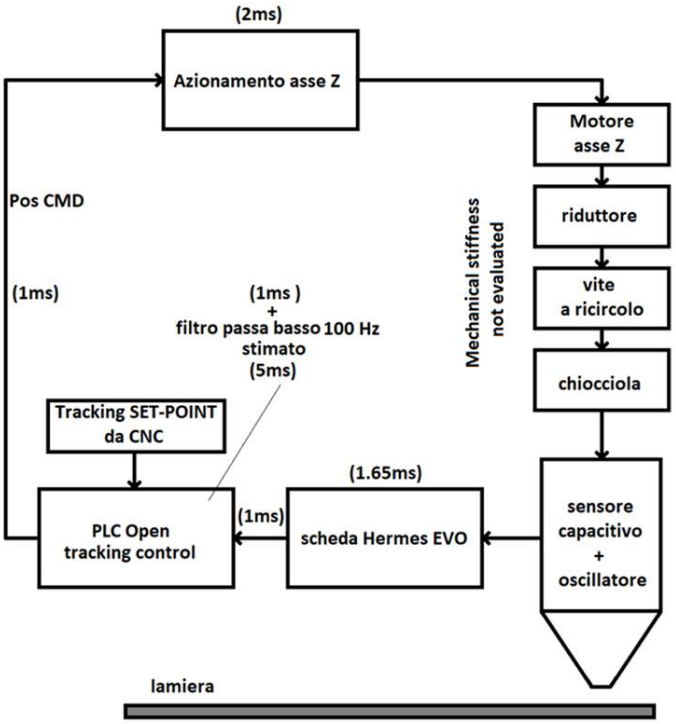

Figure 1.1: block scheme about element in the system

This estimate showed the delay to be around 10 ms. Improvement works to improve the capability of the signal tracking algorithm were proposed such as the identification and modelling of the part related to mechanical components, motor, adaptor, ball screw lead including also that cutting head so the Z - axis element.

In order to achieve the desired goal, modelling of the Z-axis was initiated by acquiring data necessary for the purpose by organising tests on the machine. In order to achieve the desired goal, tests were carried out involving the addition of white noise in order to excite the system over a wide frequency spectrum. These noises were added directly via the drive by bypassing the PLC and CN part.

The list of tests performed is given below

:

001 – Movement [0 – 100mm]

002 – White Noise – Speed Control Loop

003 – White Noise on Torque

004 - White Noise – Current Control Loop

The data acquired via the oscilloscope mounted on the machine are the calculated position input into the drive, an acquisition made only for the first test, Torque, position measured, or the position detected by the encoder mounted on the ball screw. Data acquisition involved the use of an interferometric laser to obtain accurate data with respect to the distance between the tip and the plate.

After the necessary and usual data processing, the following elements of the system were identified and modelled using the different data position.

Calculated position – Torque: Drive

Torque – Measured position: motor – adaptor

Measured position – laser position: ball screw – cutting head

The modelling followed two approaches, data - driven and first principles.

The first modelling carried out experimentally using the System Identification toolboox@Matlab as an identification tool.[2]

The need to have a model that offered scalability led to the modelling of the system using the bond graph approach, thus starting from physics. In addition, it made it possible to analyse how changing certain components of the system affect the response.

1.2 STUDY OF THE SYSTEM

1.2.1 The machine

The machine made by Prima Power is used for cutting sheet metal using a fibre optic laser. The machine under study, on which the tests were carried out, is identified as LaserGenius+.

The laser consists of a coherent beam of light whose characteristic feature is that each beam has the same wavelength. Another key element is the slider whose task is to focus the light beam at a specific point. The actual cutting takes place because of the heat that the focusing of the laser beam causes on the workpiece.

Reflection is the principle behind a fibre laser. Reflection occurs between the core (high reflective index) and the cladding (low reflective index). Incident light is reflected within the core and propagates within the fibre. The critical angle is a parameter that affects the incidence and reflection of the light beam; if the light beam hits the interface and is greater than the critical angle, the light beam will not be able to pass through the medium.

The machine consists of three axes, but from a cutting point of view, it identifies itself as a 2D machine. The reason for this is that it is only capable of cutting sheet metal in two dimensions.

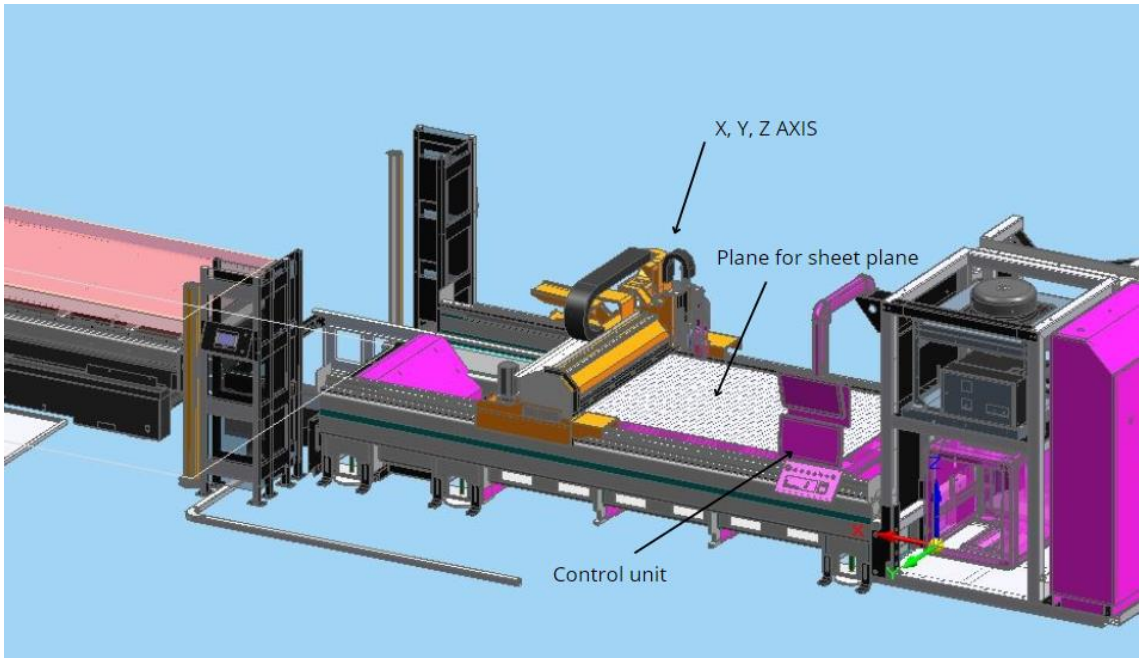

Figure 1.2: LG+ machine

The laser has different power settings, starting from 2000W up to 10000W.

The machine consists of 3 axes whose model strokes are as follows:

X: 3.150 mm

Y: 1.600 mm

Z: 150 mm

Speed and acceleration data are summarised below:

Speed:

X, Y: 130 m/min

Trajectory 180 m/min

Acceleration:

Trajectory: 2.8g

Another parameter summarising the machine's characteristics is the resolution, which for the three axes is 0.001mm.[3]

1.3 PROCESSED SYSTEM

The machine consists of three axes, but from a cutting point of view, it identifies itself as a 2D machine. The reason for this is that it is only capable of cutting sheet metal in two dimensions.

The system under study can be traced schematically as shown in the figure. The Z-axis drive consists of

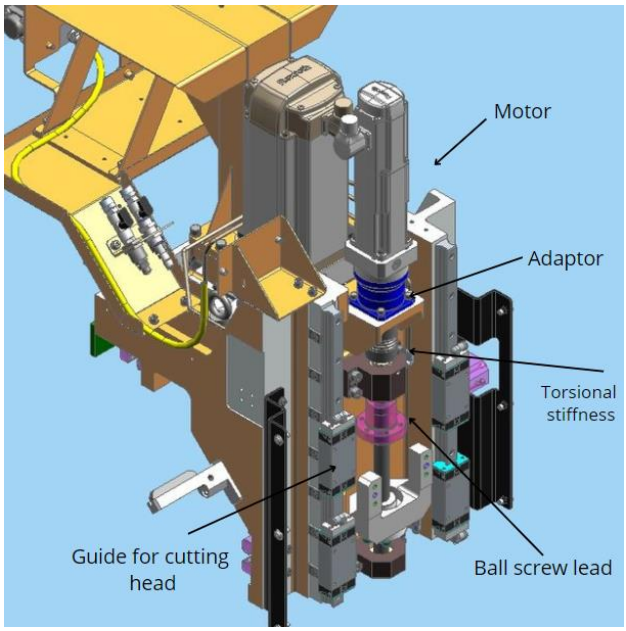

Figure 1.3: items examined

1.3.1 Drive

The drive part includes the entire control part, which in the case of the machine under consideration consists of a PI control. Included in the drive are the position, velocity and current control loops.

Due to the cascade architecture of the control loops, parameterisation is required from the innermost loop, current control loop, to the outermost loop, position control loop. For the control of the current control loop, parameter optimisation is not required in the case of a rotary motor such as the one implemented in the machine under consideration; the parameters are read directly from the encoder.

The parameters of the speed control loop depend both on motor parameters such as inertia, torques and forces, and on mechanical properties such as inertia and mass of the charge, friction and stiffness.

For the speed control loop, the parameters must be adapted with respect to jerk, acceleration and interpolation by an external speed controller.

The input signal into the drive is the commanded position (posCMD), i.e. the position that must be reached by the head in order for the sheet metal to be cut at the set distance, known as the StandOff position, in order to achieve good cutting quality even with respect to laser power.[4]

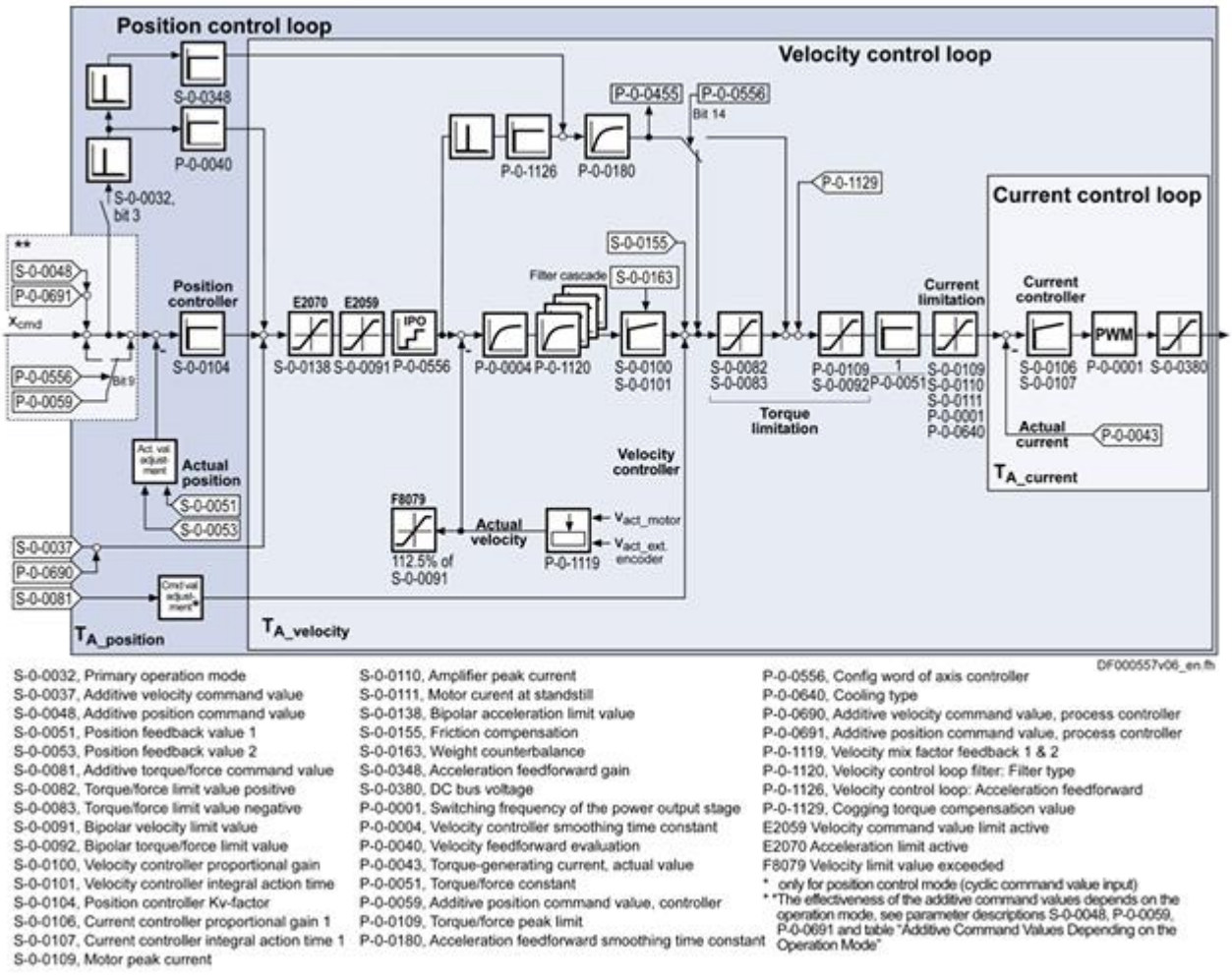

S-0-0032, Primary operation mode
S-0-0037, Additive velocity command value
S-0-0048, Additive position command value
S-0-0051, Position feedback value 1
S-0-0053, Position feedback value 2
S-0-0081, Additive torque/force command value
S-0-0082, Torque/force limit value positive
S-0-0083, Torque/force limit value negative
S-0-0091, Bipolar velocity limit value
S-0-0092, Bipolar torque/force limit value
S-0-0100, Velocity controller proportional gain
S-0-0101, Velocity controller integral action time
S-0-0104, Position controller Kv-factor
S-0-0106, Current controller proportional gain 1
S-0-0107, Current controller integral action time 1
S-0-0109, Motor peak current
S-0-0110, Amplifier peak current
S-0-0111, Motor curent at standstill
S-0-0138, Bipolar acceleration limit value
S-0-0155, Friction compensation
S-0-0163, Weight counterbalance
S-0-0348, Acceleration feedforward gain
S-0-0380, DC bus voltage
P-0-0001, Switching frequency of the power output stage
P-0-0004, Velocity controller smoothing time constant
P-0-0040, Velocity feedforward evaluation
P-0-0043, Torque-generating current, actual value
P-0-0051, Torque/force constant
P-0-0059, Additive position command value, controller
P-0-0109, Torque/force peak limit
P-0-0180, Acceleration feedforward smoothing time constant
P-0-0556, Config word of axis controller
P-0-0640, Cooling type
P-0-0690, Additive velocity command value, process controller
P-0-0691, Additive position command value, process controller
P-0-1119, Velocity mix factor feedback 1 & 2
P-0-1120, Velocity control loop filter: Filter type
P-0-1126, Velocity control loop: Acceleration feedforward
P-0-1129, Cogging torque compensation value
E2059 Velocity command value limit active
E2070 Acceleration limit active
F8079 Velocity limit value exceeded
* only for position control mode (cyclic command value input)
* *The effectiveness of the additive command values depends on the operation mode, see parameter descriptions S-0-0048, P-0-0059, P-0-0691 and table "Additive Command Values Depending on the Operation Mode"

Figure 1.4: Drive with control loop

1.3.2 Motor and adaptor

The motor receives the command from the drive as an electrical signal. The motor mounted on the Z-axis machine is a synchronous motor. The choice of this type of motor is based on the desire to have high precision and speed control without oscillations.

The torque generated by the motor is reduced by a reduction ratio via an adaptor mounted downstream of the synchronous motor. In figure is present also the torsional stiffness.

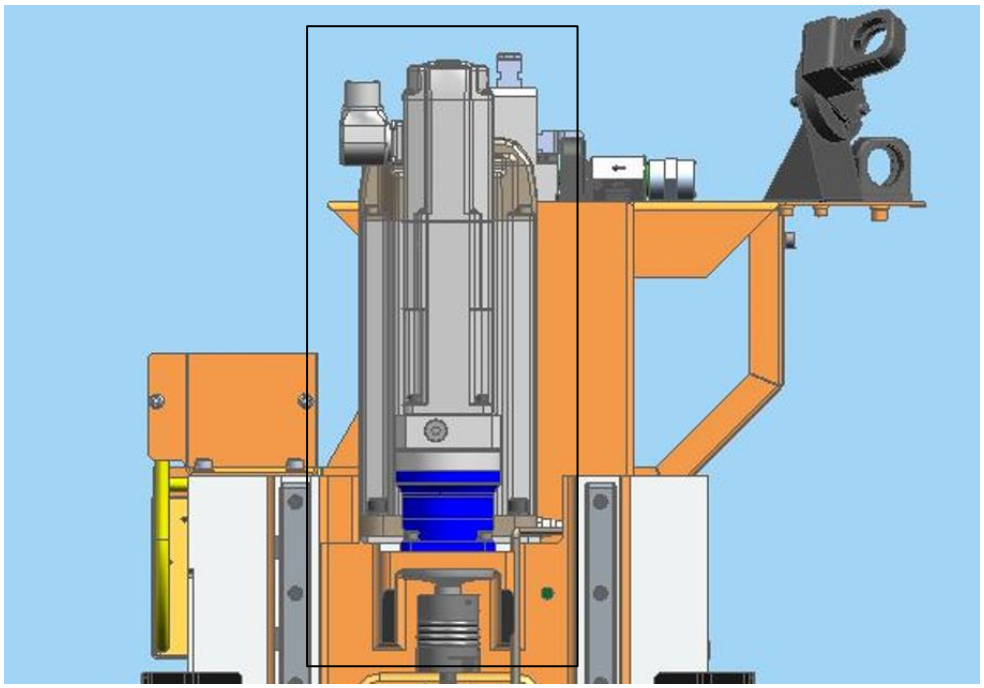

Figure 1.5: Motor, adaptor, torsional stiffness

1.3.3 Ball screw lead

A ball screw system has the task of converting rotary motion, in our case coming from a synchronous motor, into linear motion, which is the kinematics required to move the cutting head. Ball screw feeds are integrated with mechanical components to ensure high performance in terms of precision and low friction. In the machine under consideration, this system is integrated with a plate, which slides on linear roller guides. The stiffness of ball screw feed drives is the weakest in the axial direction because of the

axial and torsional stiffness of the screw shaft, as well as the flexible kinematic joint, including the support bearing and ball screw pair. The linear guideway only plays a guiding role in the transmission direction. The uniaxial static and dynamic models commonly assume that only the axial deformation of rolling interfaces and screw shafts occurs. The assumption ignores the moment effect caused by the misalignment between the screw shaft axis and the loading position. Compared to the figure below, the system is mounted vertically, coinciding with the direction of the Z axis.

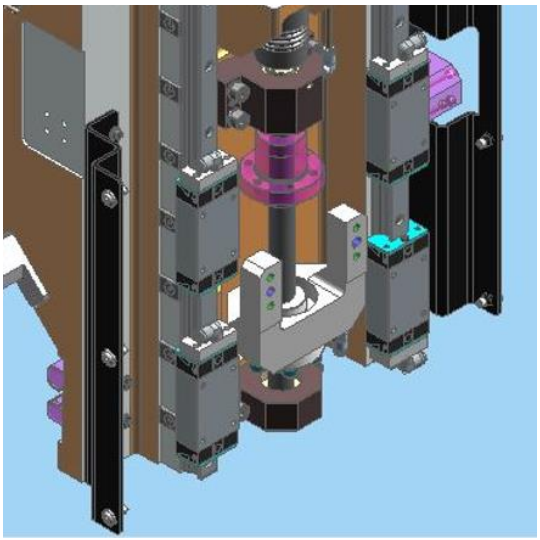

Figure 1.6: Ball screw lead

1.3.4 Cutting head

The collimator fixed by a ball screw via four guides that allow it to move vertically. The optical path of the machine is constituted by an optical fibre cable which guides the laser beam from the generator, through the X chain system, the Y chain system and the Z chain system to the collimator. From the collimator, the laser beam, through the mirrors of the head, is sent to the focusing lens.

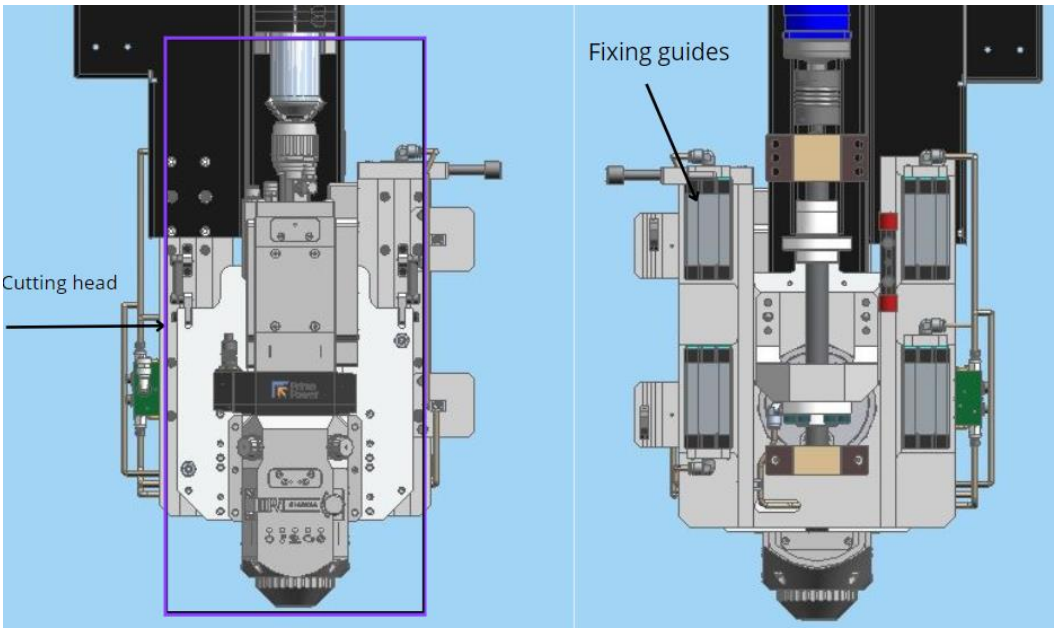

Figure 1.7: Cutting head system (left). Rear view (left)

2 MODELLING APPROACHES

2.1 Introduction

When approaching system modelling, we encounter two primary approaches: First principles (White box Approach) and Data-Driven Modelling (Black-Box Approach).

System identification is a fundamental discipline that empowers us to construct mathematical models of real-world systems or signals by analysing observed data. These mathematical models have evolved into indispensable tools in modern science and engineering, serving a diverse range of purposes, including simulations, predictions, control system design, and signal processing. Mastering various modelling techniques is therefore essential for navigating these complexities.[5]

First Principles (White Box Approach)

If the underlying physical laws governing the real-world system are known, we can exploit this a priori knowledge to construct the model. This approach is referred to as physics-based modelling or simply modelling. Here, we utilize the fundamental principles of physics, such as Newton's laws, thermodynamics, or fluid dynamics, to develop equations that describe the system's behaviour. This method relies on our understanding of the mechanisms and interactions within the system, enabling us to create detailed and accurate models. However, developing these models can be complex and time-consuming, particularly for systems with intricate interactions or those influenced by a wide range of variables. The primary advantage of the white-box approach is its transparency and interpretability, as the models derived from first principles often provide deep insights into the system's functioning.[6]

Data-Driven Modelling (Black-Box Approach)

In contrast, if the system's physical details are obscure but we have access to measured data, we can utilize this data to build the model. This approach is known as data-driven modelling or simply identification. In black-box modelling, we do not assume any prior knowledge about the system's internal mechanisms. Instead, we use statistical and machine learning techniques to infer the system's behaviour directly from the data. Methods such as regression analysis, neural networks, and support vector machines are commonly employed to identify patterns and relationships within the data. The strength of the black-box approach lies in its flexibility and applicability to a wide range of systems, even those with complex and unknown dynamics. However, these models often lack interpretability and may not provide insights into the underlying processes driving the system.[7], [8]

Hybrid Approaches (Grey – box approach)

In practical scenarios, we often possess only partial information about the system's physics. This calls for a hybrid approach that combines a priori knowledge with experimental data to construct the model. This hybrid modelling approach leverages the strengths of both white-box and black-box techniques, enabling us to effectively capture the system's dynamics even with limited information. Hybrid models can take various forms, such as grey-box models, where certain parameters are estimated from data while others are based on physical laws, or ensemble methods that integrate multiple models to improve accuracy and robustness. By blending physical insight with data-driven methods, hybrid approaches can provide a more comprehensive understanding of the system and enhance predictive performance.[9], [10]

System identification provides a powerful framework for constructing mathematical models of real-world systems, enabling us to understand, predict, and control their behaviour. Whether we rely on physics-based knowledge, data-driven approaches, or a hybrid combination, system identification remains an essential tool for engineers and scientists across various disciplines.

The significance of system identification extends beyond mere model construction. In control system design, accurate models are crucial for developing controllers that ensure desired performance and stability. In signal processing, system identification techniques help in filtering, denoising, and feature extraction from observed data. Moreover, in fields such as economics, biology, and environmental science, system identification enables the analysis of complex, dynamic systems where direct experimentation may be impractical or impossible.

Advancements in computational power and algorithms have further propelled the capabilities of system identification. Machine learning has revolutionized data-driven modelling by providing sophisticated tools for handling large datasets and uncovering intricate patterns. Techniques such as deep learning and reinforcement learning have opened new avenues for modelling highly complex and nonlinear systems, from financial markets to autonomous vehicles.

Nevertheless, the choice between first principles and data-driven approaches is not always straightforward. Each approach has its strengths and limitations, and the optimal choice often depends on the specific characteristics of the system and the available information. For instance, in well-understood physical systems with clear governing laws, first principles modelling might be preferable. Conversely, in systems where the underlying

physics are too complex or unknown, data-driven methods may offer a more viable solution.

System identification is a cornerstone of modern engineering and science, providing the means to construct models that elucidate the behaviour of real-world systems. By leveraging the power of mathematical modelling, whether through first principles, data-driven methods, or hybrid approaches, we can gain deeper insights, make accurate predictions, and devise effective control strategies. As technology advances and our understanding of complex systems grows, the role of system identification will continue to expand, driving innovation and progress across diverse fields.[11]

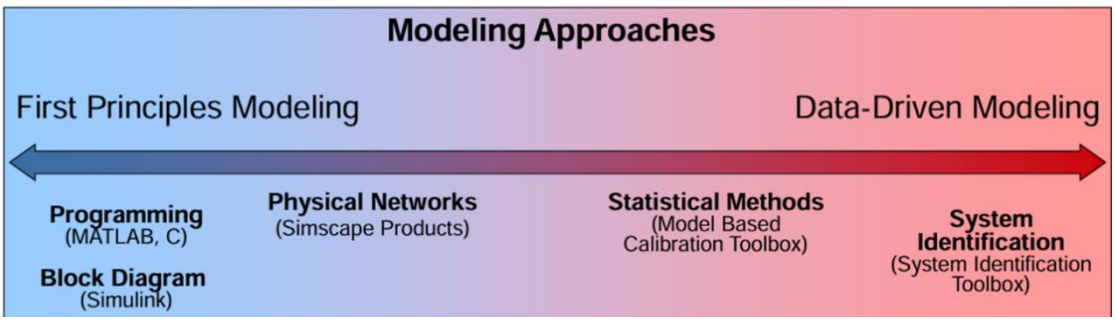

Figure 2.1: Modelling approaches

2.2 Data – driven approach

System Identification allows the construction of a mathematical model from the data. The model describes the relationship between the measured signals; for this reason, it is essential to divide the signals into input and output. Black-box modelling is useful when your primary interest is in fitting the data regardless of a particular mathematical structure of the model. The toolbox provides several linear and nonlinear black-box model structures, which have traditionally been useful for representing dynamic systems. These model structures vary in complexity depending on the flexibility you

need to account for the dynamics and noise in your system. You can choose one of these structures and compute its parameters to fit the measured response data. Black-box modelling is usually a trial-and-error process, where you estimate the parameters of various structures and compare the results[12], [13], [14]. Typically, you start with the simple linear model structure and progress to more complex structures. You might also choose a model structure because you are more familiar with this structure or because you have specific application needs. In case of estimate linear parameters, it used a transfer function that represent a ratio of polynomials:

$$G(s)=\frac{(b_0 + b_1 s..)}{(1 + f_1 s..)}$$

A commonly used method for these identifications, ARX (AutoRegressive eXogenous input model) processes by least squares (LS) using discrete data and a direct approach, was used to estimate the transfer function.

An autoregressive model is a type of statistical model that represents a time series as a linear combination of its past values. It is represented by the equation below:

$$(p^n + a_1 p^{n-1} + a_n)\, y(t) = (b^1 p^{n-1} + b_n)u(t) + e(t)$$

Where p is the operator for differentiation, y(t) is the output and u(t) the input. It is including also the source of white noise.

The estimate parameter vector is:

$$\theta = (a_1, a_n b_n, b_n)^T$$

The LS approach often can lead to very low mean square errors of parameter estimates particularly for a small sampling period. [15], [16].

When a linear model provides poor fitting with respect to the measured output signals and the same result is obtained even when changing the model

order, non-linear models may be required. Non-linear models have greater flexibility in capturing complex phenomena than linear models of similar order. This approach was used to identify the components between the input torque in the motor and the measurement taken by the encoder, which is positioned on the screw. The components between these two measurements are the motor, gearbox, coupling and elastic coupling.

Data-driven modelling was performed using a MATLAB toolbox called *System Identification Toolbox*. This tool provides MATLAB functions that allow dynamic systems to be modelled, analysed and worked on data sets, and predictions to be made. For our purpose, it was used to estimate transfer functions from the measurements taken and to estimate the dynamics of non-linear systems such as motor - adaptor modelling.

2.2.1 Hammerstein-Wiener Models

The Hammerstein and Wiener models are special kinds of nonlinear systems where the nonlinear block is static and follows or is followed by a linear system. These models have applications in many engineering problems and therefore, identification of Hammerstein and Wiener models has been an active research area for many years. [17]

For systems where the output exhibits a non-linear relationship with the input, it's sometimes possible to break down this complexity. We can accomplish this by decomposing the input-output relationship into interconnected elements. This allows us to represent the system's dynamics using a linear transfer function, while capturing the non-linearities with separate functions applied to the input and output of the linear system. The Hammerstein-Wiener model achieves this by connecting static non-linear blocks in series with a dynamic linear block.[17], [18]

The Hammerstein-Wiener model itself consists of a series structure. It includes input and output non-linear blocks flanking a central linear block. This linear block, typically represented by a discrete transfer function, captures the system's dynamic behaviour.

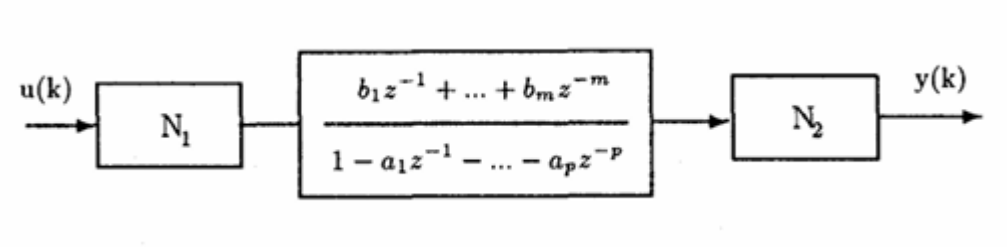

Figure 2.2: Hammerstein - wiener models

The function f linked the nonlinear input, transforms given input *u(t)* to $w(t) = f(u(t))$. The size of the output of this equation is equal to the input and represents the input for the linear block. The linear block is composed of the equation below $x(t) = \frac{B}{F}x(t)$. Also, in this case the dimension of the output is the same as the dimension of the input. B and F are polynomials in linear Output - Error (OE). OE models are polynomial models that can correlate inputs and outputs from measurements. It has been a model used for our purposes since it also includes white noise as a noise.[19], [20].

$$y(t) = \frac{B(q)}{F(q)}u(t - nk) + e(t)$$

Polynomial estimation can be performed in time domain, as in this case, or in frequency domain. After the order of the polynomial is defined, n input variables and n output variables are considered. With the number of samples *nk*, corresponding to the delay-dead time of the input, given by the number of samples before the output responds to the input The non-linear block is composed of the equation $y(t) = h(x(t))$ where the block transforms the output by the configuration, in this case piecewise.

2.3 First principles approach

2.3.1 Introduction

In modelling electromechanical systems, the first principles approach is widely used. In this part of the paper, we have focused on modelling the Z-axis from the physics of the system. The decision to also model the system using this type of approach stems from the need to develop a model that allows us to change the components in the system and assess how their variation affects the output responses.

The first principles approach differs from the previous one in its ability to represent physical phenomena by exploiting physical laws to describe the system's dynamics. In electromechanical systems, this approach is advantageous as there are several iterations between electrical and mechanical components in different domains.[21]

2.3.2 Bond graph

The presence of different domains within the system has driven modelling towards a tool based on the exchange of energy flows within a system, the Bond Graph. This methodology makes it possible to describe the different energy domains and their iterations. To obtain a comparison with data-driven modelling, the components were modelled considering the data obtained from the machine test. [15][16]

The choice of considering energy exchange as a model variable leads to considering for each domain two variables indicated as effort and flow from which the following energy relationship is obtained:

$$E = e \cdot f \, dt$$

Effort means those variables such as force, voltage, pressure, and flow the variables velocity, current and flow rate. Energy is transformed through ports that represent energy communication interfaces. There are four energy interfaces:

Energy source: The inputs to the system, which represent a convenient way of defining a constraint on the modelled system, to determine its reaction to stress or flow stimuli.

Energy store: These elements store the effort and flow variable. They are described as effort or flow stores.

Energy dissipation: these are elements that allow energy to be dissipated into the environment. An example of these elements can be in the electrical domain the resistance.

Energy transfer elements: These elements store energy, merely routing the energy through the model, between any other elements in the model. In some energy domains these elements are well defined (e.g. parallel connections in electrical systems), while in others are more abstract (common strengths in mechanical systems). mechanical). Included in this group of elements are couplers that neither store nor dissipate energy but transform stress and flow variables without and flow variables without energy loss.

Domain	effort	e	flow	f	momentum	p	displacement	q
electric	e.m.f.	e	current	i	lines	λ	charge	q
magnetic	m.m.f.	M	flux rate		-	-	flux	ϕ
hydraulic	pressure	P	volume flow rate		pressure momentum	p	volume	V
mechanics translation	force	F	velocity	V	momentum	P	displacement	x
mechanics rotation	torque	T	angular velocity	ω	angular momentum		angle	α
thermo-dynamics	temperature	T	entropy flow rate		-	-	entropy	S

Table 2-1: Domain and element about BG

The link between the various elements is represented by the junctions, which allow the components to be connected and define which of them behave as integrative elements and which as derivative elements. There are mainly four types of junctions. Element "0" has at least two ports and represents the relationship between elements that share the same effort and is called common effort.

Another element which can be called the dual to the previous one is the common flow indicated by the symbol "1" which shares the same flow with the other elements. In this case, too, it consists of at least two ports.

Transformers are designated by "TF" nodes in bond graphs and are again power conserving although the effort on the output port is scaled by the transformer ratio to the effort on the input port.

Finally, the last junction is the Gyrator designated by "GY" which is another power-conserving element that directly bonds the flow input and effort output, and vice versa. This element is used in the presence of transducers between different energy domains.

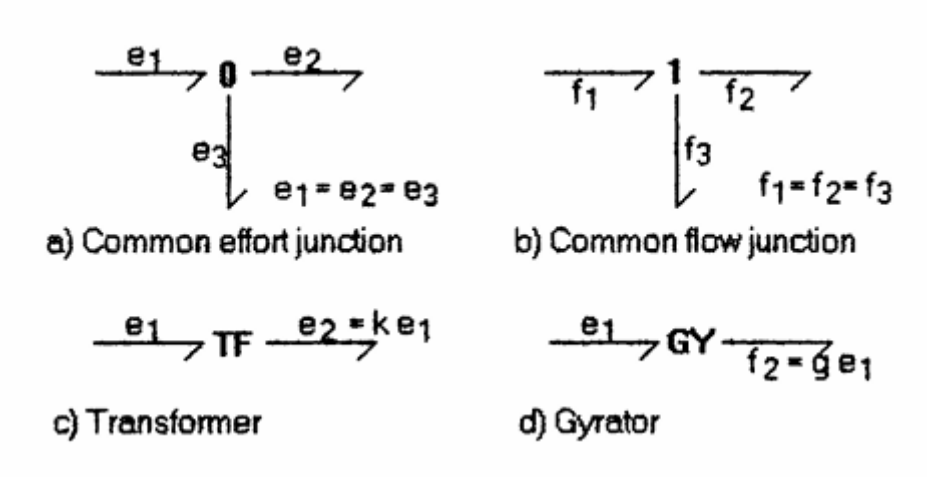

Figure 2.3: BG junction elements

As already said, the elements constituting the bond graph fall into three main categories: energy source, energy stores and energy dissipator. The symbols and the relative constitutive equations of the bond graph elements that were also used for modelling during this discussion are shown below. Each element is then linked, according to the desired domain, to the component to which it refers.

Symbol	Element Type	Constitutive Relation
SF ⟶	Flow Source	$f = f_{in}$
SE ⟶	Effort Source	$e = e_{in}$
⟶ C	Flow Store	$e = 1/C \int f\,dt = q/C$
⟶ I	Effort Store	$f = 1/I \int e\,dt = p/I$
⟶ R	Dissipator	$e = R.f$ or $f = e/R$

Table 2-2: BG symbols and constitutive equations

In order to conclude the discussion of the constituent elements of the bond graph, it is necessary to define how the casualty between the elements is defined in order to represent the dynamics of the system. By causality is meant the transformation of the graphical representation into an equation of

state linked in this case to an integral type of casualty. In assigning casualty, an attempt is made to maximise the states of the system, i.e. to obtain as many integrative states as possible. Once the casualty has been defined, and consequently what the integrative and derived states are, the equations defining the system are obtained from the constitutive relations.[22], [23]
The assignment is made based on the knowledge and behaviour of the system. The energy source elements impose their state on the system so that their casualty is known a priori

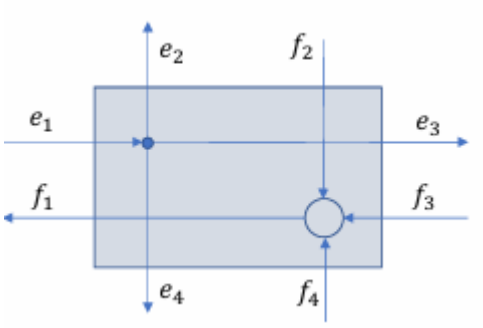

Figure 2.4: 0 - junction

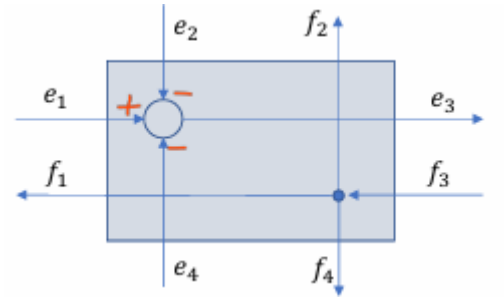

Figure 2.5: 1 junction

On the left-hand side is the casualty referred to the 0 junction, where effort is the output for one component and becomes input for all others. In contrast, 1 junction shown on the right, the flow is output from one component while the others are seen as input.
Once the equations of state of the system have been obtained, the state space is created according to the relation:

$$\dot{x}(t) = A\,x(t) + B\,u(t)$$
$$y(t) = C\,x(t) + D\,u(t)$$

The state representation after obtaining the matrices was used to represent the system and compare it with what was obtained through data-driven modelling.

3 IDENTIFICATION PROCEDURE

3.1 Introduction

The identification process involved carrying out several tests on the LG+ machine, with the aim of obtaining meaningful data to better identify the Z-axis components. The data available following the movement of the axis was taken from the oscilloscope present directly on the machine, which is able to record the parameters coming from the sensors mounted on the axis, parameters coming from the drive and from the numerical control. An initial modelling activity relating to the mechanical components involved using the data acquired from the oscilloscope relating to the position of the encoder and the commanded position, i.e. the target command that the drive sees as input before performing the tuning operations within the three control loops. This first data-driven identification only identified the motor - gearbox and nut part. The cutting head, which is attached to the nut via a plate with skids, was not optimally identified, as the only data relating to the head's displacement relative to the sheet metal was recorded by the capacitive sensor, whose position value is shown as the commanded position indicated earlier.

3.2 Interferometric laser

In order to improve identification, the part of the system whose data recorded by the oscilloscope did not fully represent the head-to-plate distance.

To solve this data gap, a measuring instrument used for calibration and to correct any measurement errors on CNC machines was used, the interferometric laser. This measuring instrument uses a coherent beam of

light, which is split into two identical beams by an interferometer and consequently follows two different paths. The two beams come together before reaching the detector. The difference in the distance of the path followed by the beams creates a phase shift, which can be constructive or destructive. Signal processing is carried out by the detector, which can observe the interference of the beam. The interference loop proves a continuous, cyclic variation in the intensity of the assembled beam. The intensity variation occurs when the reflected measurement shifts by 316.5 nm, which is precisely half the wavelength of the laser. The displacement is measured by the relationship between the wavelength λ, and the number of cycles passed. d= (λ N)/2 [nm]. The accuracy achieved by this measuring instrument is 1nm

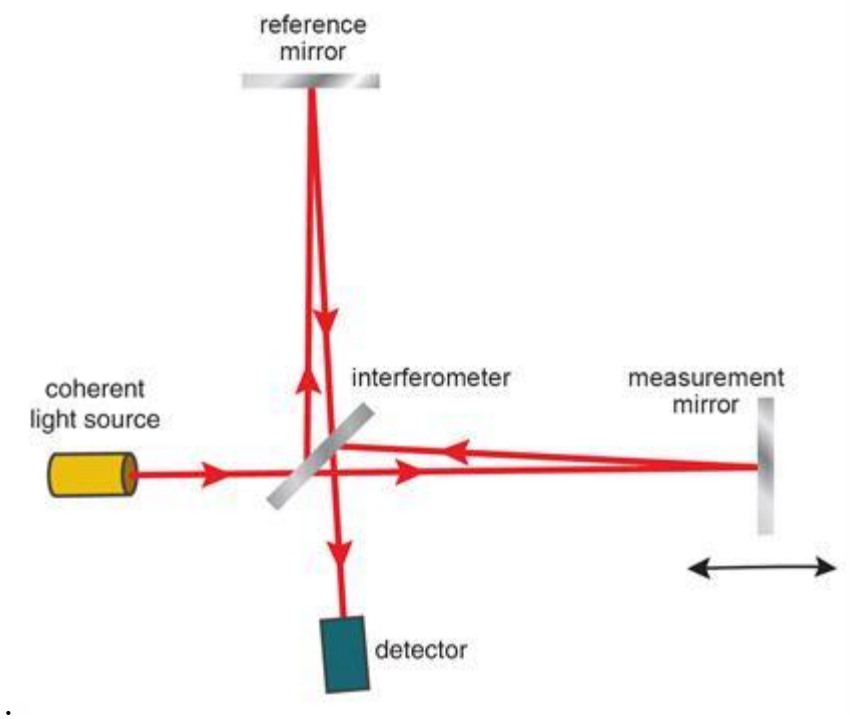

Figure 3.1: Interferometric laser

The purpose of the tests performed on the machine was to simulate the behaviour of the system, specifically the movement of the cutting head.

In order to collect more data during the identification phase, tests were carried out to excite the system over a wide frequency range.

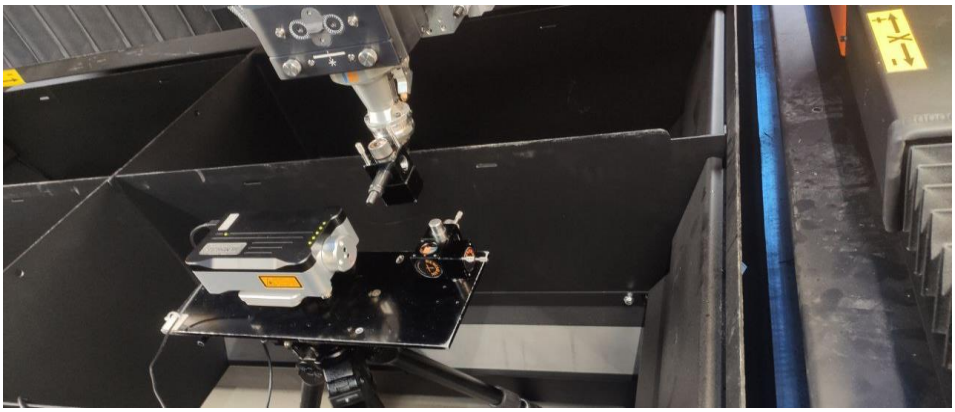

Figure 3.2: interferometric laser and collimator during acquisitions

To achieve this, the use of white noise is a very common practice in engineering specifically for system identification.

The use of white noise finds its benefit in generating signals with a constant power spectral density over all frequencies, thus obtaining frequencies that have equal power. Frequency response analysis makes it easy to identify natural frequencies, damping factors. For the project, this type of test was used to obtain information with respect to system properties such as masses, stiffnesses and damping. Another benefit of using white noise to excite a system, rather than a simple sine wave, is because the latter can have a frequency equal to the natural frequency of the system, a situation that causes oscillations and vibrations of the entire machine, affecting, in our case, the quality of the cut. White noise prevents this phenomenon by considering all excitation frequencies within it.

The identification carried out is called open loop identification. The system is directly perturbed by a signal chosen by the user without any feedback effect.

Figure 3.3: Identification flow

3.3 Test bench

The machine on which the tests were carried out is part of the Laser Genius + 2040 series, whose abbreviation indicates the size, in width and length respectively, of the machinable sheet metal. The Z axis moves on two guides in X and Y in a bridge configuration.

The motor manufactured by Bosch Rexroth and the gearbox manufactured by Wittenstein have the following specifications:

Motor Inertia	4,40E-05	kgm^2
Adaptor Inertia	4,000E-06	kgm^2
Acceleration Torque	3,005	N
Static Torque	0,531	N
Motor revs	6000	rpm
Motor weight	2,4	Kg
Gear ratio	3	\

Table 3-1: motor – adaptor datasheet [24]

Downstream of the adaptor, in order to compensate for axial misalignments, vibrations of which play an important role during the cutting process, there is torsional joint with a torsional rigid flexible coupling with the following characteristics:

Nominal Torque	16	Nm
Angular misalignment	1°	deg
Torsional stiffness	11	Nm/rad
Moment of inertia	0,05	kgm2

Table 3-2: Torsional joint datasheet

The conversion of the motion from rotary to longitudinal, which allows the head to move along the Z axis, is entrusted to the ball screw lead. The ball screw lead is the element that is mounted on the screw which allows the transfer of motion to the flange. The characteristics of the screw and nut are summarised in the table:

Screw pitch	40	mm
Screw inertia	3,06E-05	kgm2
Screw revs	20000	rpm
Screw displacement	13,33	\
Static load factor	26200	N
Dynamic load factor	14000	N

Table 3-3: Ball screw datasheet[25]

For physical modelling, no stiffness values for the system described are available from datasheets. The literature and manufacturers' catalogues provide an approach for estimating the stiffness.

The total axial stiffness depends on the component parts, which in this case are the screw and nut and the bearings:

$$\frac{1}{k_{bs}} = \frac{1}{R_{fb}} + \frac{1}{R_s} + \frac{1}{R_{nu}}$$

- k_{bs} – total stiffness
- R_s – screw stiffness
- R_{nu} – nut stiffness

However, for the estimation of the total stiffness, some considerations suggested by the manufacturer's catalogue were made. In practice, the screw stiffness is substantially lower than the nut stiffness. The total stiffness value considered is equal to:

$$R_{bs} = 380 \cdot 10^6 \ \frac{N}{m}$$

3.4 Test performed

The following is the procedure and type of tests performed. The identification of the system by means of machine tests was performed by dividing the tests into two parts.

The first test carried out was aimed at performing a rigid identification of the system; to this end, a low-frequency test was performed. Elastic phenomena, on the other hand, are related to high frequencies, in fact, the second type of tests performed present higher system excitation frequencies.

The white noise added via the drive with the "Signal shape selection" function, which allows

In order to improve the data processing and analysis phase, Trigger Waves were provided, so as to have references between the data coming from the oscilloscope and the data coming from the interferometric laser from the point of view of data alignment. Trigger waves, as well as having a different waveform to those provided for the individual tests, were not considered in the identification procedure.

1st test

The first test consists of having the head perform a movement from [0 - 100 mm]. During this test, the feed rate was set to 100% and the number of movements performed by the head was three.

The trigger wave: square wave [0 - 1mm] with a feed rate of 5%.

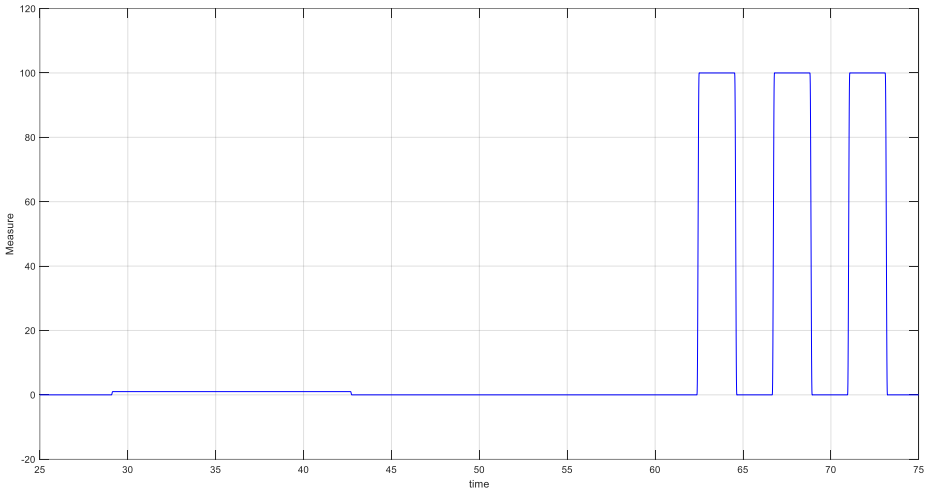

Figure 3.4: first test with trigger wave

2nd test

Subsequent tests on this basis are aimed at identifying rigid dynamics. The excitation of the system was done by adding a white noise directly to the speed control loop. The addition of the noise on the control loop was done by acting directly on the drive, modifying the parameters by bypassing the PLC part of the system, and CN also performed for the subsequent tests.

Adding the white noise at this point of the control had the purpose of exploiting the dependence of the control on the mechanical parameters Also in this case a trigger wave was provided: Sine Wave [period T= 2s; amplitude A=10 rpm].

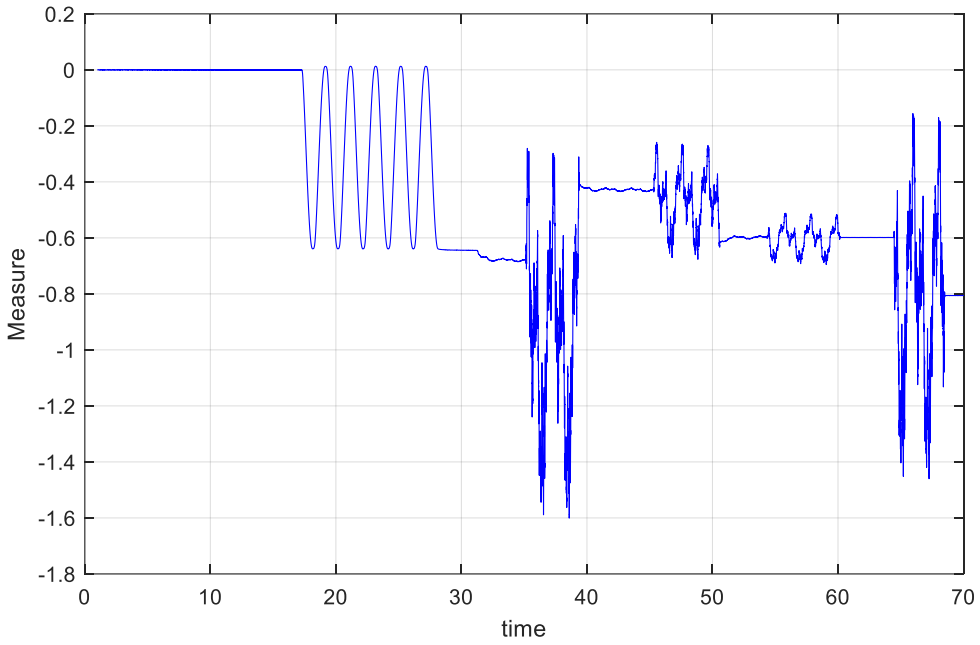

Figure 3.5: second test with trigger wave

3rd Test

The logic used for the third test is similar to the previous one. In this case, the excitation of the system by means of white noise was carried out with the addition of the disturbance on the torque; thus, the part of the system relating to the axis electric motor is disturbed.

Trigger wave: Sine Wave [period T= 2s; amplitude A=10 rpm].

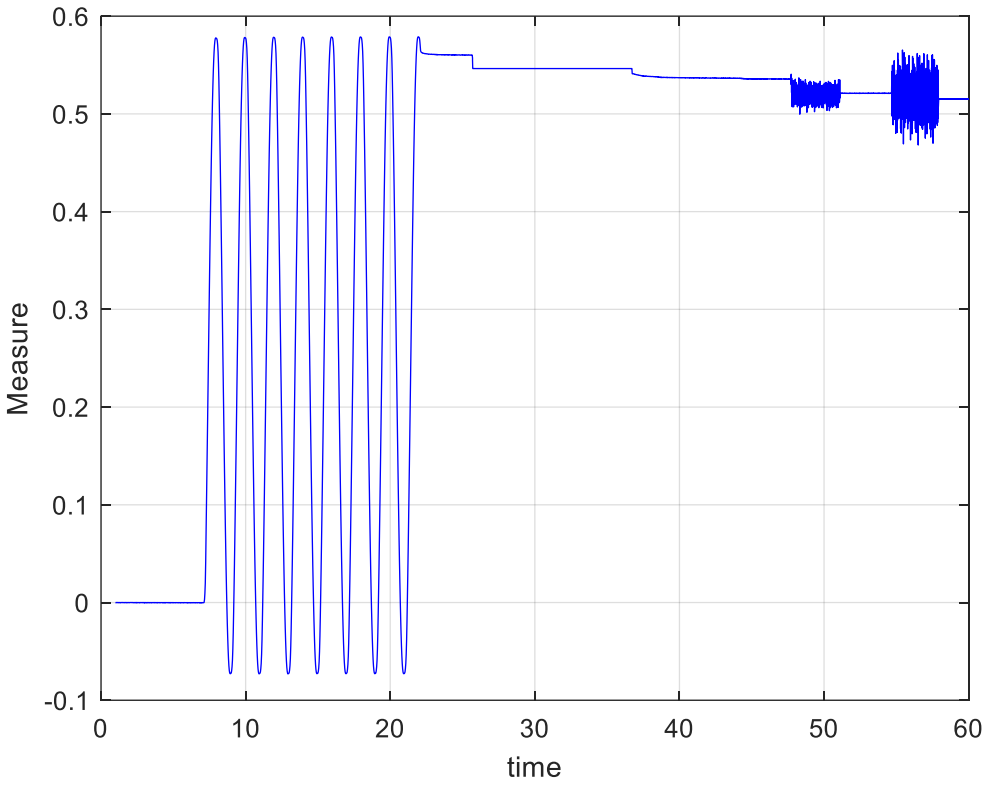

Figure 3.6: third test with trigger wave

4th Test

In the last test performed, white noise was inserted into the current loop. In this case, the waveform generated to which the noise was added were two square waves with the following characteristics:

T= 50%, 0.2 mm RISE EDGE, 0.2mm FALL EDGE

T=100%, 0.2mm RISE EDGE, 0.2mm FALL EDGE

Trigger wave: Sine Wave [period T= 2s; amplitude A=10 rpm].

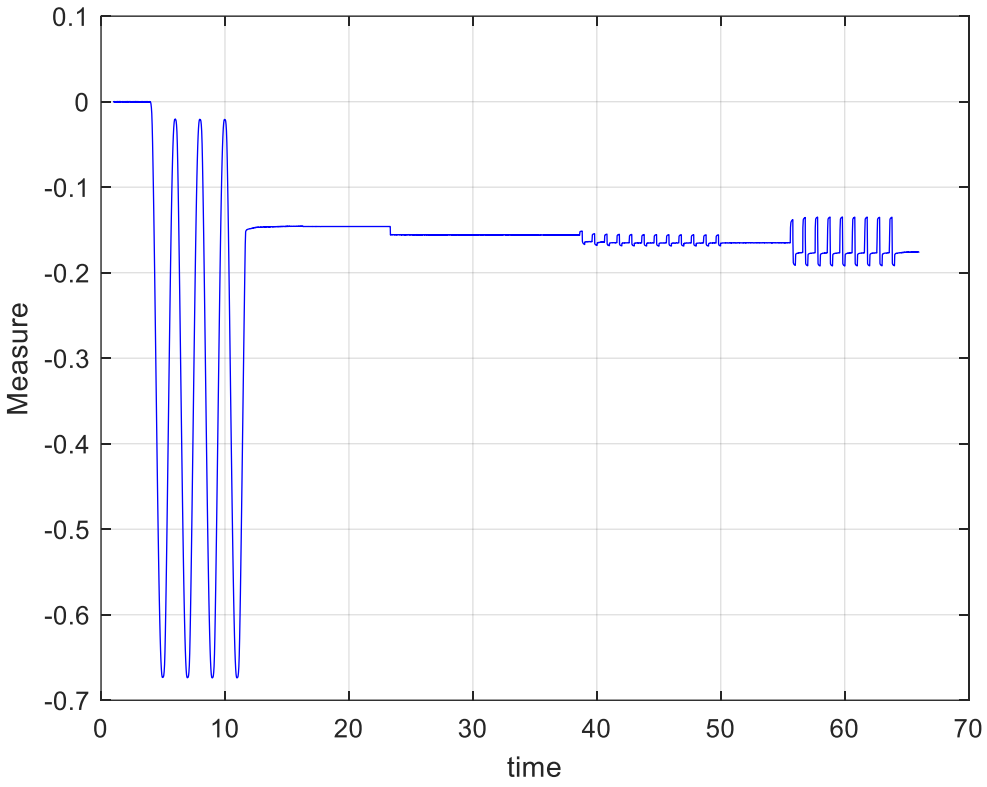

Figure 3.7: fourth test with trigger wave

4 DATA PROCESSING

The data collected during the tests were chosen in such a way that component identification could be carried out. The acquisition frequency of the oscilloscope is 1kHz and a sampling time of 1 ms. This data was used as a reference for processing the data from the oscilloscope, which had a different acquisition frequency. For this purpose, three parameters were recorded from the oscilloscope on the machine:

- Calculated physical position
- Measured physical position
- Z Torque

The acquired data were saved imported as a .csv file and pre-processed with MATLAB. The data was initially saved as a matrix using the readmatrix(xx.csv) function. The data was then associated with the variables useful for our purpose. The variables saved are:

- Time
- Measured_pos
- Calculated
- Torque

This was done for each of the four tests.

The time vector was normalised in such a way as to obtain a time vector starting from 0 with a sampling time of 1ms; this operation was necessary because the acquisition by the oscilloscope and by the laser had different durations and sampling times using the linspace function.

For the two position measurements, however, these were not absolute. The oscilloscope records position relative to the machine zero, so it was necessary to subtract the first value of the vector from each element in order to bring the position measurement in line with the desired output.
The new time vector, comparable in length with the laser time vector, was used to interpolate via the interp1 function, the measured position and the calculated position.

The measurement from the laser was acquired using the CARTO software, an application supplied by the measuring instrument manufacturer as a .mat file. As mentioned earlier, the instrument's acquisition frequency is 50kHz. The oscilloscope has an acquisition frequency of 1kHz, so pre-processing was also necessary for this data. This process was carried out in MATLAB. Resampling of the data was done using the resample function, the data required for which were, the measurement, the current frequency (50kHz) and the desired frequency (1kHz). The new variable was saved and exported to the calculation file for comparison with the oscilloscope measurement. The operation was performed in the same way for all tests performed. The alignment of the various curves was done using the trigger wave inserted into the test for this very purpose. The find function made it possible to find in the measured position vector and the laser vector, the values at which the curve changed course and was taken as a reference for aligning the signals.
A comparison of laser and oscilloscope measurements divided by test is shown below.

001 – Movement [0 – 100mm]

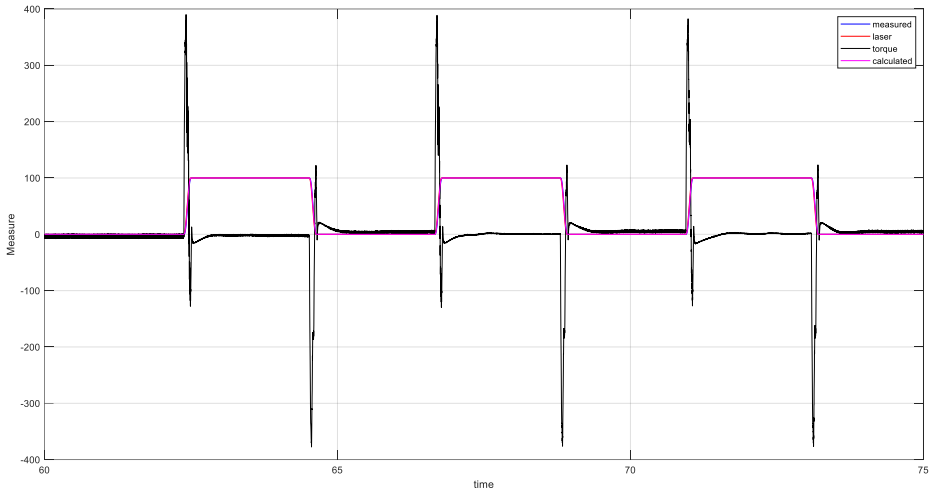

Figure 4.1: data acquired 1st test

In the figure, torque values are shown in black. At the peak value (400 Nm) there is the rise edge positive, an instant in which the cutting head reaches, and maintains, the 100mm position. The head returns to the initial position (0mm) at the change in torque value (-400 Nm). The values for the measurement from the laser, the encoder (measured position) and the input measurement in the drive (calculated position) are shown in the figure below.

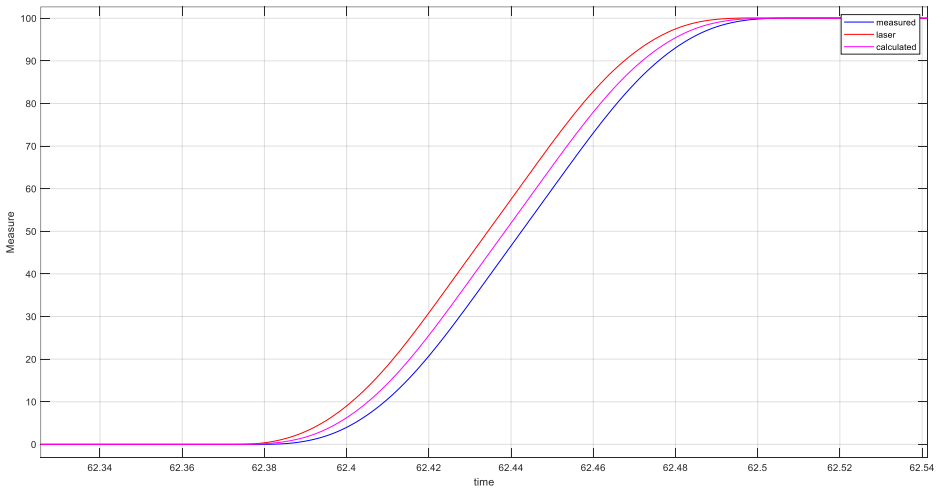

Figure 4.2: analysis position signal

The laser, also due to its acquisition frequency, detects the change in head position immediately. The delay present with the other curves can be estimated at 1 ms equal to the measurement of one sample. This value was considered during data-driven identification.

002 – Movement with White Noise – Speed Control Loop

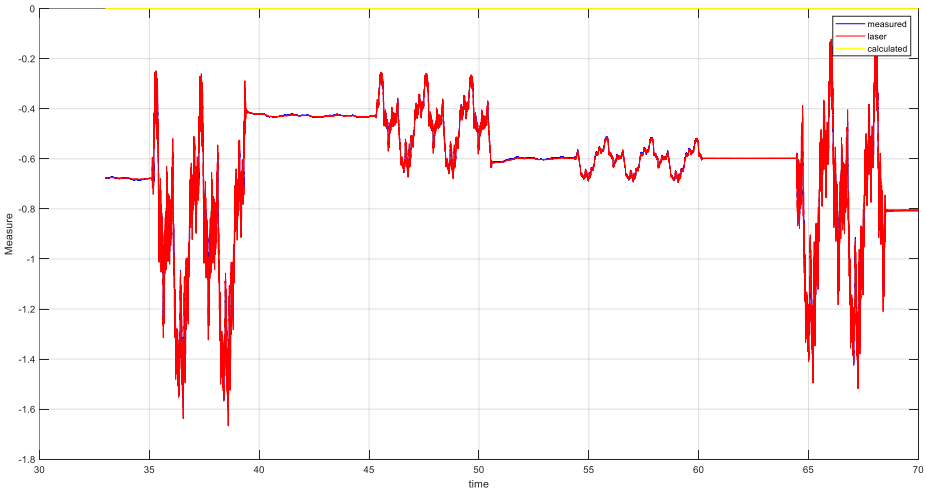

Figure 4.3: data acquired 2nd test

In the second test performed, a fast movement of the cutting head was performed in order to simulate a cutting process. Using the drive, white noise was added to the speed loop to have a wide range of excitation frequencies for the system. As can be seen from the picture, four Z-axis movements were performed. You can see that in the wing part of the graph, the calculated position has a constant value and does not vary with the laser and encoder measurement. This is because the movement was induced and disturbed directly by the drive, thus bypassing the CN and PLC part. A wave zoom is performed in the figure below.

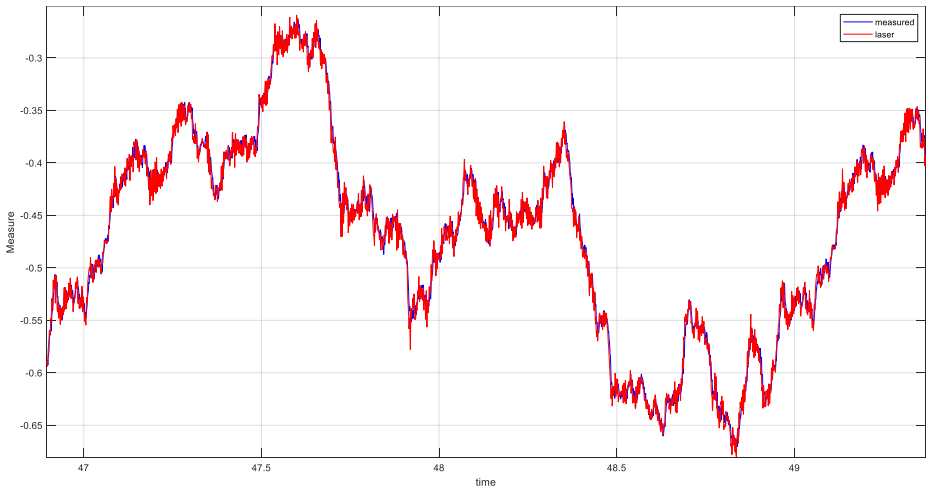

Figure 4.4: zooming second movement in test

The figure refers to the second movement of the axis in second test. The interferometric laser measurement is able to capture more information about the axis movement than the encoder. In fact, when the axis movement is larger, the encoder performs more accurate tracking as can be seen in the figure below.

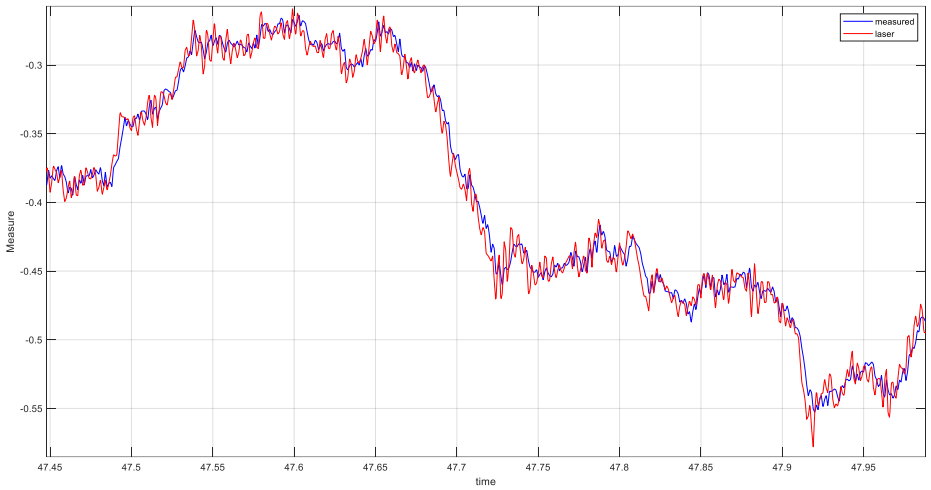

Figure 4.5: Comparison encorder_laser position

The presence of white noise, which causes rapid oscillations of the head at certain times, is not detected by the encoder. However, the presence of damping elements and high stiffnesses lead to the filtering of movements that could cause oscillations during normal operation, having an impact on cutting quality.

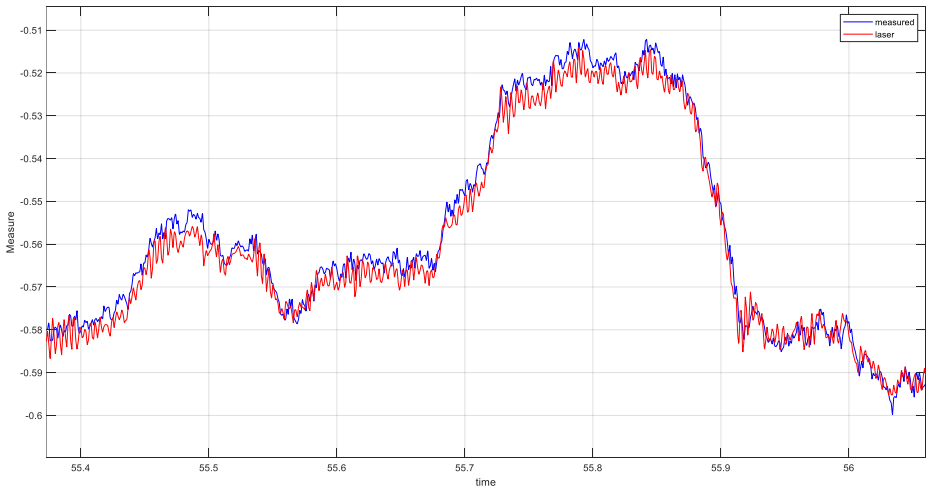

Figure 4.6: Comparison with low amplitude

The figure refers to the third set of axis movements. In this case, the amplitude is reduced. As mentioned earlier, in this case there is not only a sampling delay but also a measured position shift.

The differences noted confirm how excitation by means of a white enables the mechanical components to be estimated by means of an identification process.

The torque trend is shown in the figure.

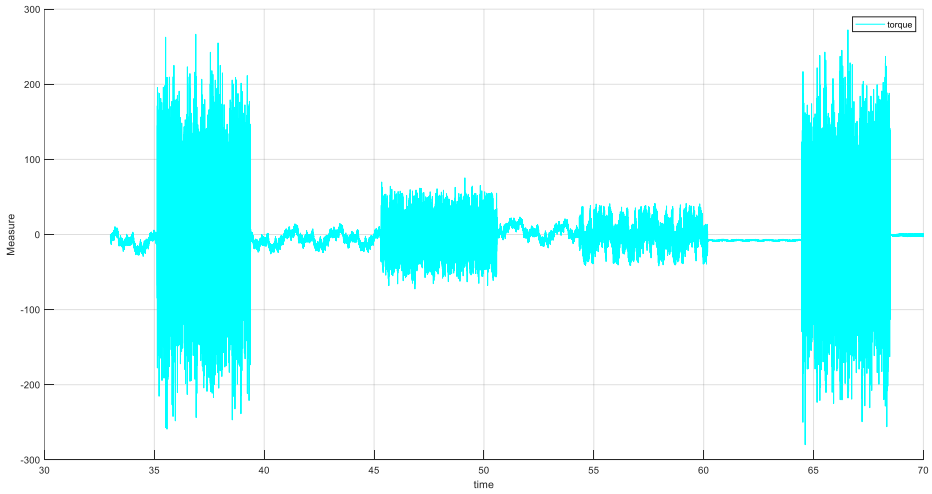

Figure 4.7: Torque about second test

003 – Movement with White Noise on Torque

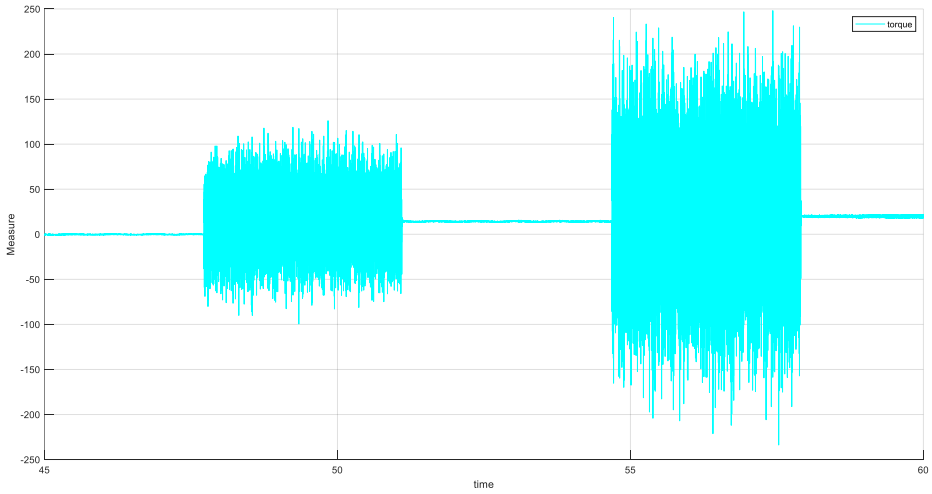

Figure 4.8: Torque 3rd test

In the 3rd test, white noise was added to the torque. The aim of adding noise to torque is to correctly identify the part of the system between the torque and the encoder measurement, i.e. motor - gearbox. The range of torque values is comparable to the previous tests. There are two movements performed by the axis with different amplitudes.

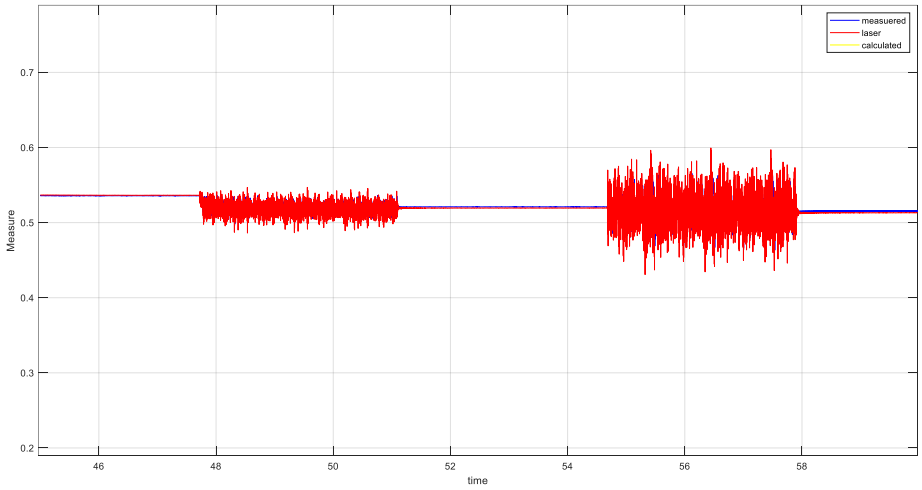

Figure 4.9: position data 3rd test

As in the previous test, the calculated position does not feel any displacement due to the reasons explained in the previous test. Also in this case, the axis performs two different movements between the two acquisitions. In the second, the measured position better follows the course that the laser measurement performs. In any case, this test was used for non-linear toolbox system identification.

004 – Movement with White Noise – Current Control Loop -

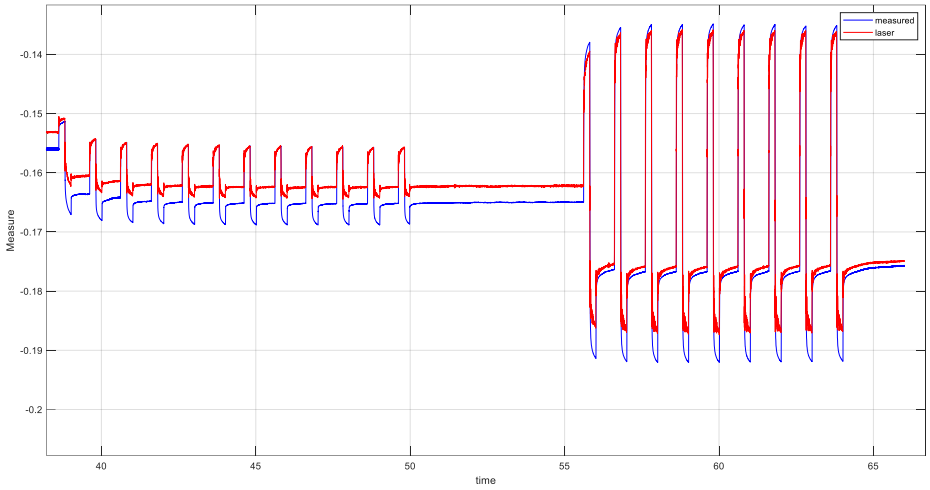

Figure 4.10: encoder laser position 4th test

In the 4th test, white noise was added to the current control loop. In this case, the addition of the noise influences the measurement revealed by the encoder. In fact, despite the alignment of the signals by means of the trigger wave (see figure below), when white noise is added, there is a shift in the curves. The shift is more evident for the acquisition with a smaller amplitude in agreement with what was also the case for the other tests.

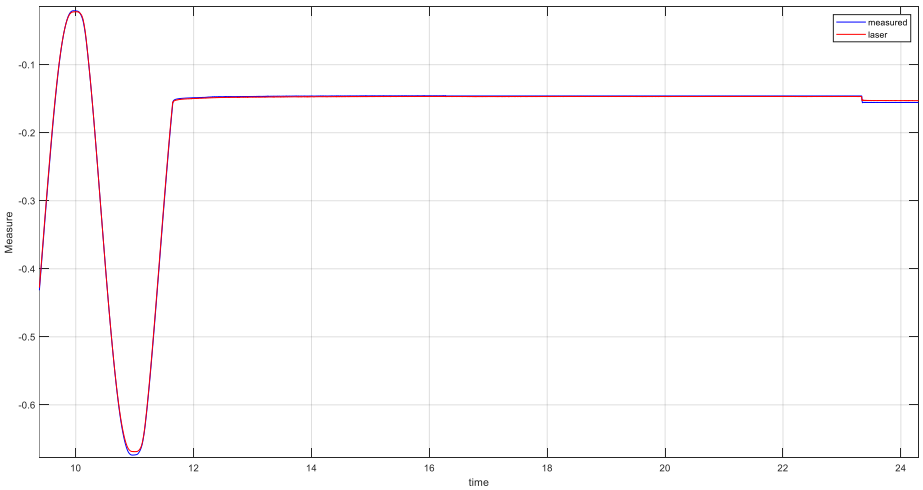

Figure 4.11: Alignment with trigger wave

In the figure, one can see the sine wave where the curves are aligned and the beginning of the phase shift at the same time as the white noise enters around 23s.

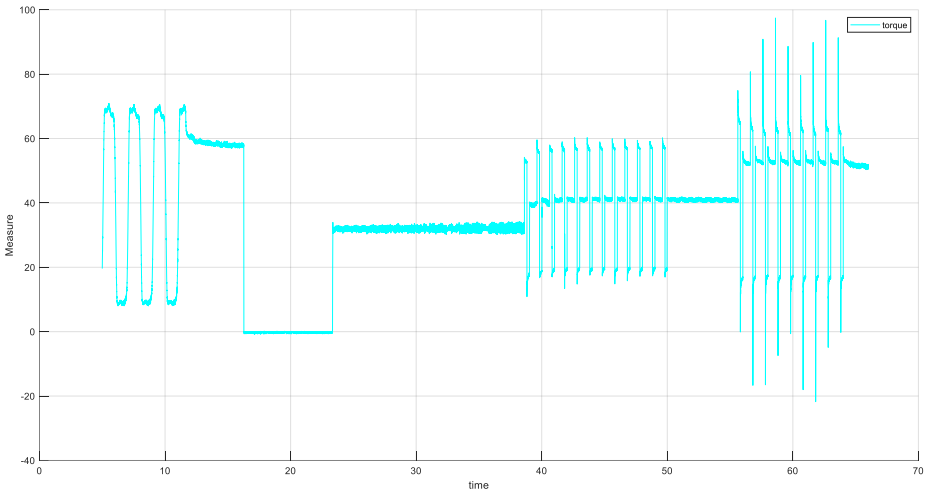

Figure 4.12: Torque 4th test

The effect of white noise on the current control loop is also noticeable for torque. In the figure, torque is also present relative to the trigger wave. Around 23s, white noise enters, and the torque measurement becomes disturbed. The link between the current loop and torque is due to the fact that the electric motor receives voltage as input, which is transformed into torque with the motor's characteristic Kt, so the relationship between them is direct. Recalling the torque trend in the first test, square wave-like movements were also performed in this case. The torque trend is similar but with more noticeable peaks due to the disturbance. The test was deepened for motor identification purposes.

4.1 Data analysis

4.1.1 Introduction

The identification of a system is an iterative process in which different models are identified from different data ranges until the model that best describes the system's dynamics is found.
The identification process begins with the import of data from the worksheet. The representation of the data in the toolbox can be done as an object or as a frequency representation. For representation as an object, the function iddata was used. Use the *iddata* object to encapsulate input and output measurement data for the system you want to identify. System identification functions use these measurements to estimate a model. Model validation functions use the input measurements to provide the input for simulations, and the output measurements to compare how well the estimated model response fits the original data.

iddata objects can contain a single set of measurements or multiple sets. Each set of data corresponds to an experiment. The data were represented in the time domain with the following code:
data = iddata (y, u, Ts)
creates an iddata object containing a time-domain output signal y and input signal u. Ts specifies the sample time of the experimental data.

Figure 4.13: Data on System Identification toolbox

For each test performed, as seen, several acquisitions were made with different axis movements. The imported data was separated in order to reduce the number of samples and separate the estimation part and the validation part. The data, once isolated, were analysed for offset, linear trend, delay and their behaviour in time and frequency. The available measurements allow an identification of the individual components. Specifically, in addition to the separation of the individual movement data, the data object with input e output referred to the modelling component:

- Calculated position – Torque: drive
- Torque – Measured position: motor – adaptor
- Measured position – laser position: ball screw – cutting head

4.1.2 Calculated position – Torque: Drive

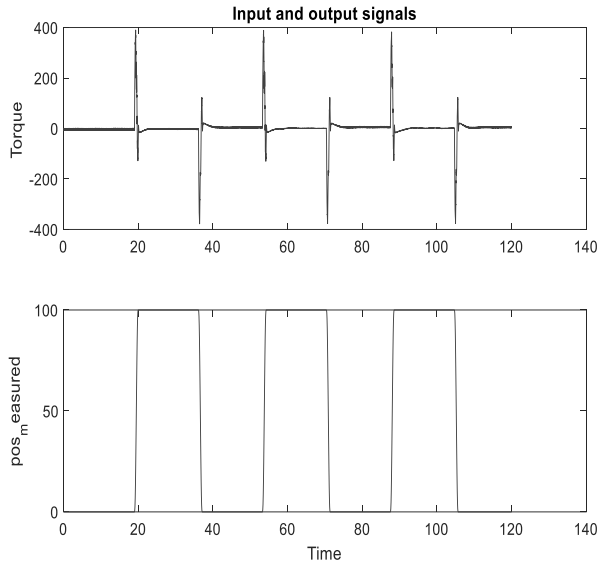

Figure 4.14: drive identification data

For the first component to be identified, the drive, the signals available are the position coming from the CN while the torque (at the top in the figure) is considered at the output of the drive. The first test is the only one among the tests performed where information on the calculated position was acquired. In this test, there are no disturbances added.

4.1.3 - Torque – Measured position: motor – adaptor

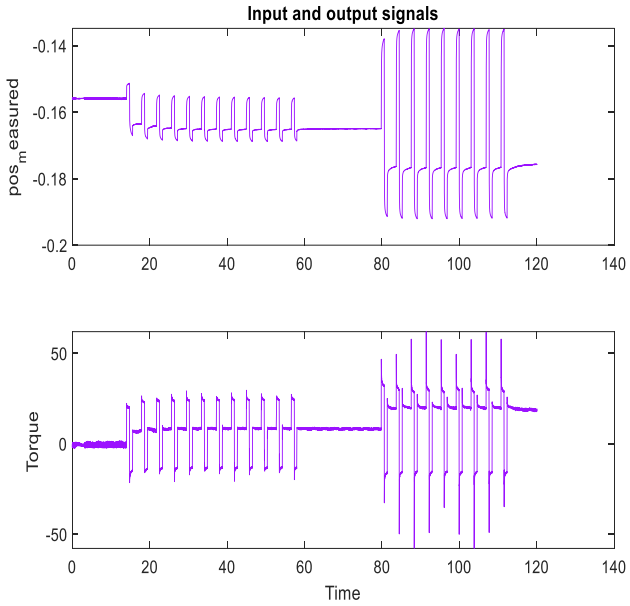

Figure 4.15: motor adaptor identification data

In the trend in the figure, torque is taken as input. The test referred to in the graph is the 4th test. In this test, the disturbance added to the current loop is intended to identify the part between the measured position, i.e. the measurement from the encoder seen as output in this case, and the torque. The elements present refer to the mechanical components of the motor including the gearbox and the elastic coupling.

4.1.4 - Measured position – laser position: ball screw – cutting head

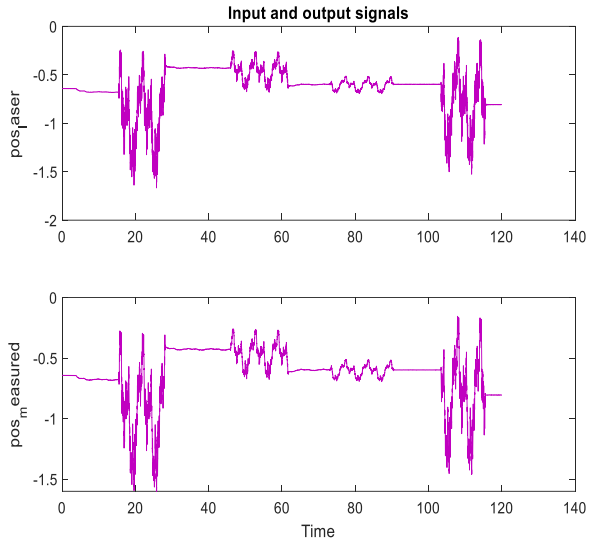

Figure 4.16_ BS - cutting head identification data

The last element of the axis to be identified is positioned between the measured position, in this case intended as input, and the measurement from the interferometric laser, i.e. the laser position entered as output for identification purposes. The test in the figure refers to the 3rd test where the disturbance for the excitation of the system was added to the speed control loop to better highlight the mechanical elements closer to the load.

After importing the data, we proceeded to pre-process the data using the tools within the toolbox. The movements in each test were isolated and categorised using the range function by entering the object in the working data tab. The purpose of the division was to have data sets to be used as model estimation and others as validation.

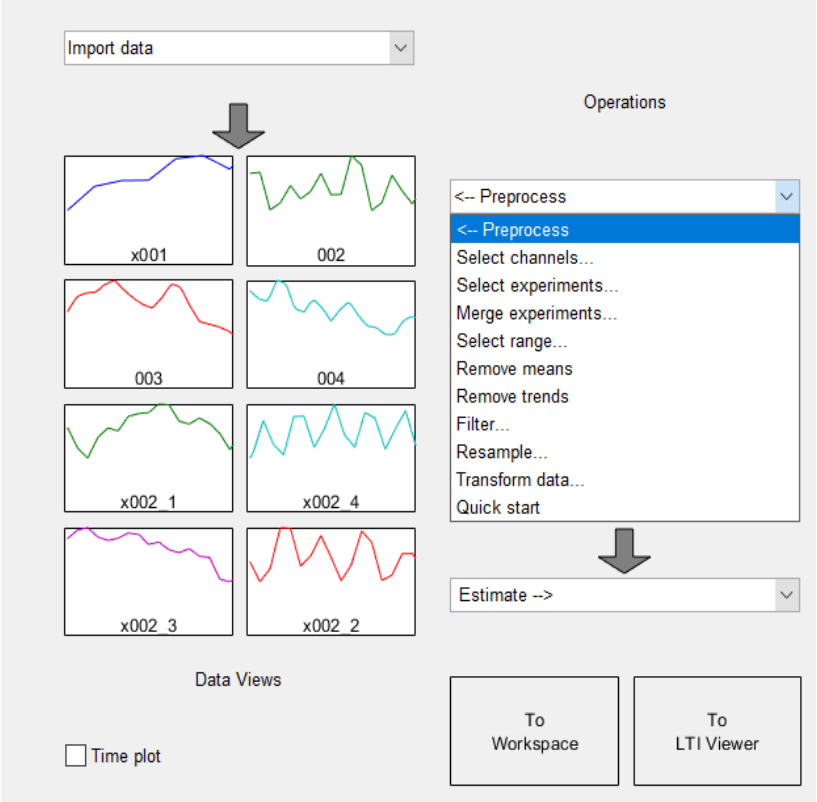

Figure 4.17: Pre -elaboration data on toolbox

The isolation of the data made another data processing operation necessary. In fact, the data in their entirety considered relative movements Detrending operation is removing means, offsets, or linear trends from regularly sampled time domain input-output data signals. This data processing operation helps you estimate more accurate linear models because linear models cannot capture arbitrary differences between the input and output signal levels. The linear models you estimate from detrended data describe the relationship between the change in input signals and the change in output signals. For steady-state data, you should remove mean values and linear trends from both input and output signals.

5 Data – driven identification

5.1 Introduction

After the pre-processing of the data, we moved on to the estimation of the models. The estimation of models is the main part of the *SystemIdentifcation Toolbox*. From the Estimate window, it is possible to proceed with the modelling from the working data. Estimation is basically divided into two categories:

Direct estimation of the Impulse or the Frequency Response of the system. these methods are often also called nonparametric estimation methods, and do not impose any structure assumptions about the system, other than that it is linear.

Parametric methods. a specific model structure is assumed, and the parameters in this structure are estimated using data. This opens a large variety of possibilities, corresponding to different ways of describing the system. Dominating ways are state-space and several variants of difference equation descriptions.

To obtain linear models, considering the nature of input and output data for component identification, the transfer function was used. To generate the tf it is necessary to provide the number of poles and zeros, presence of input or output delays in the form of samples, and the selection between discrete time and continuous time.

The iterative process led to the evaluation of different combinations of poles and zeros. Specifying a higher model order for the same linear model structure. Higher model order increases the model flexibility for capturing complex phenomena. However, unnecessarily high orders can make the model less reliable. The evaluation was initially done by checking the fitting between the generated model and the dataset used as validation.

The operation the app performs refers to the following command: *tfest(data,2,1)*.

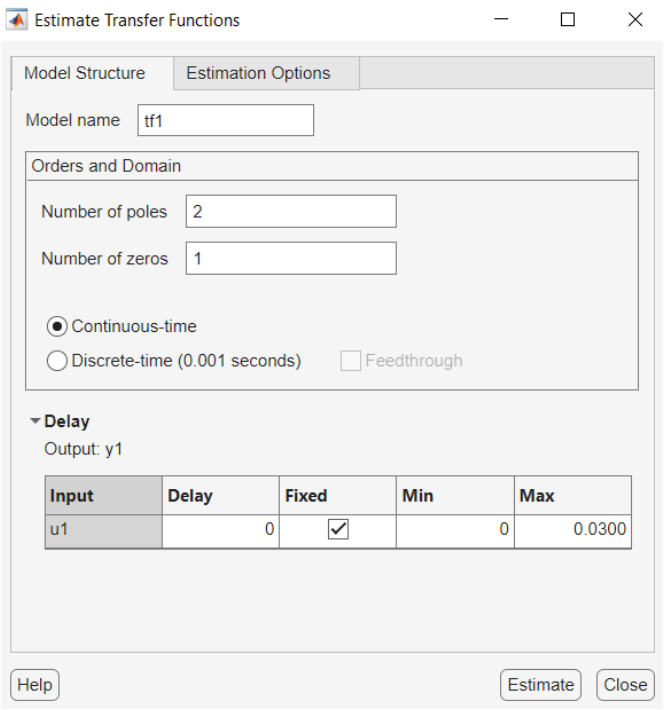

Figure 5.1: Transfer function estimation

5.2 Drive identification

The identification of the drive starts from the position signal and as output is the torque signal processed by the controller. A range of the validation performed is shown in the figure. The plots show the simulated (predicted) outputs of selected models. The models are fed with inputs from the

Validation Data set, whose output is plotted in black. In time domain, as in this case, the simulated or predicted model output is shown together with the measured validation data. In all the cases, the percentage of the output variations that is reproduced by the model is displayed at the side of the plot and a higher number means a better model. The precise definition of the fit is:

$$fit = \frac{(1 - norm(y - \widehat{y}))}{norm(y - mean(y))} \cdot 100$$

Where y is the output while $\widehat{y}$ is the predicted output. In this case the fitting is 87.22%.

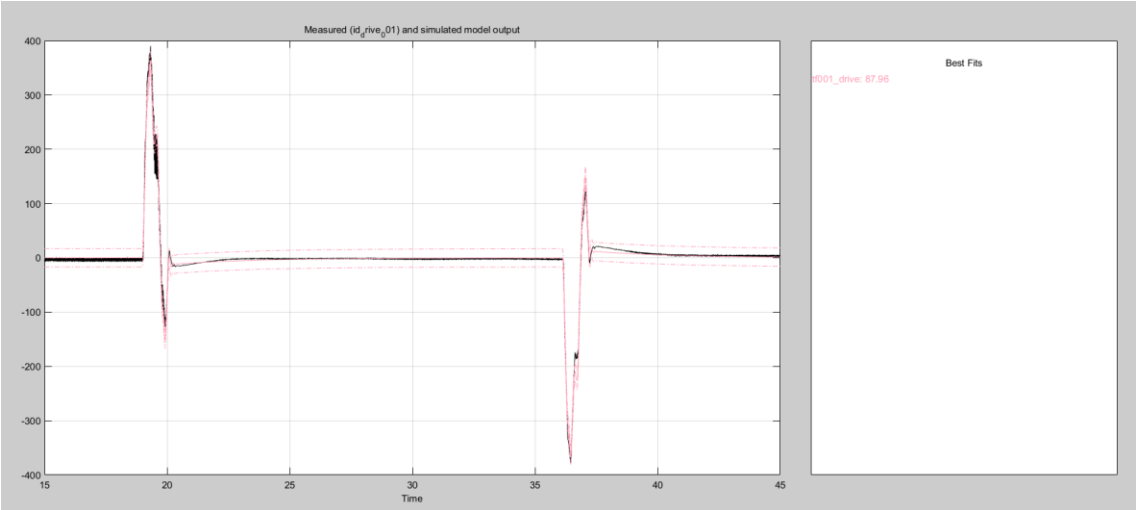

Figure 5.2: drive identification output

Any estimated model has a degree of uncertainty, which affects the reliability of the various model properties. Therefore, all model views have estimated accuracy measures. The uncertainty region is marked by two dash-dotted lines, one on either side of the nominal model curve with the same colour as the curve. The statistical interpretation is that (with the indicated probability) the true system response is found within the marked confidence region. This interpretation assumes that the system can be described within the chosen

model class and that the model has passed validation tests. In this case the test in passed in fact the pink line in inline of the confidence region.

```
From input "Calculated_position" to output "Torque":
619.4 z^-1 - 1238 z^-2 + 619 z^-3
---------------------------------
  1 - 1.994 z^-1 + 0.9941 z^-2
```

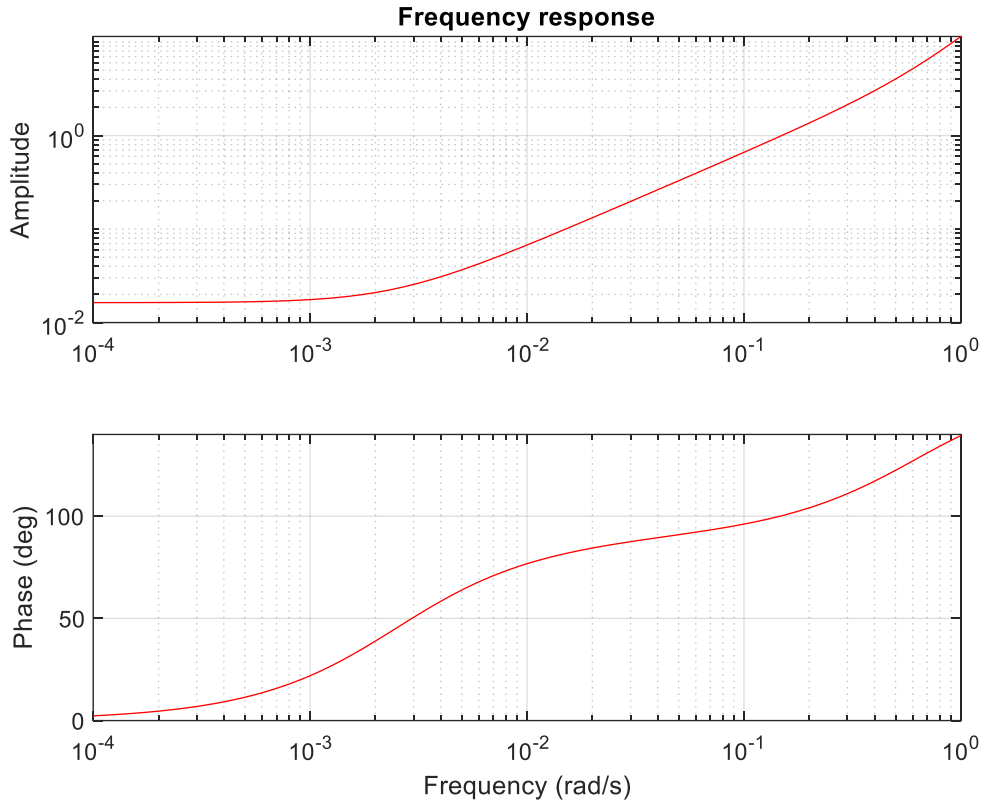

Figure 5.3: frequency response tf

The transfer function consists of 3 poles and 2 zeros. The identified system has a linearly increasing response with increasing frequency. This behaviour is typical of a system that amplifies signals with increasing frequency.

$$p_1 = -0{,}9970 + 0{,}0076j \ \frac{rad}{s}$$

$$p_2 = -0{,}997 - 0{,}0076j \ \frac{rad}{s}$$

$$p_3 = 0 \ \frac{rad}{s}$$

$$z_1 = 0\ \frac{rad}{s}$$

$$z_2 = 0.993\ \frac{rad}{s}$$

The phase, on the other hand, shows an increasing phase delay with increasing frequency, which can be linked to integrative behaviour. Considering that the identification carried out relates to a drive in which, as seen, the 3 control loops are present, the analysis of the tf and bode diagram matches the system identified.

Current control loop must have a very fast response in order to provide immediate control via the current to be supplied to the motor. In terms of bandwidth, however, we can say that this is generally high.

Velocity control loop is responsible for controlling and stabilising the speed of the motor. Its bandwidth is lower.

The bandwidth for the position control loop is the lowest of the three. Analysing the denominator of the *tf*, there are complex poles near the unit typical of position and velocity control systems with damped oscillatory behaviour.

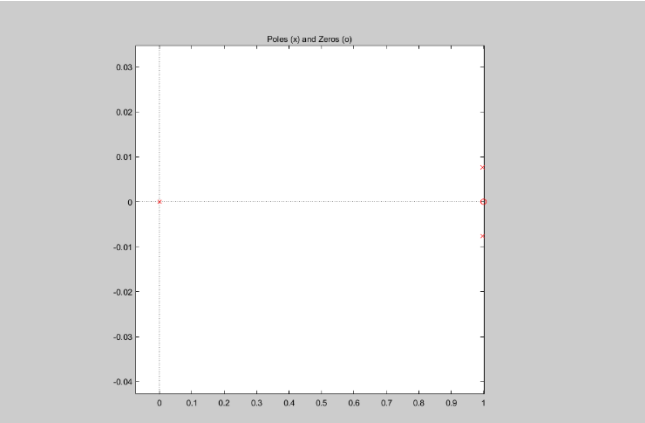

Figure 5.4: zeros and poles position

In terms of stability, the position of the poles and zeros were analysed.
The poles are close to the unit circle suggesting that the system is stable. The position of the zeros has an influence on the frequency response but does not directly affect the stability of the system.

5.3 Motor – adaptor identification

For the second element in the system consisting of the motor and the gearbox. The signals available are the torque of which we therefore consider the mechanical part, the torque reducer and the elastic coupling, the purpose of which was clarified in the last chapter. The non-linearity of the signals between input and output made it impossible to identify the system by means of a transfer function. The approach used led to the use of a non-linear identification method also found in the toolbox called Hammerstein-Wiener. In this identification method, there is an alternation of non-linear blocks referring to the input and output signals and a linear block between the two. For the modelling of this component using this non-linear method, it was first necessary to indicate a non-linear data set referring to Torque.

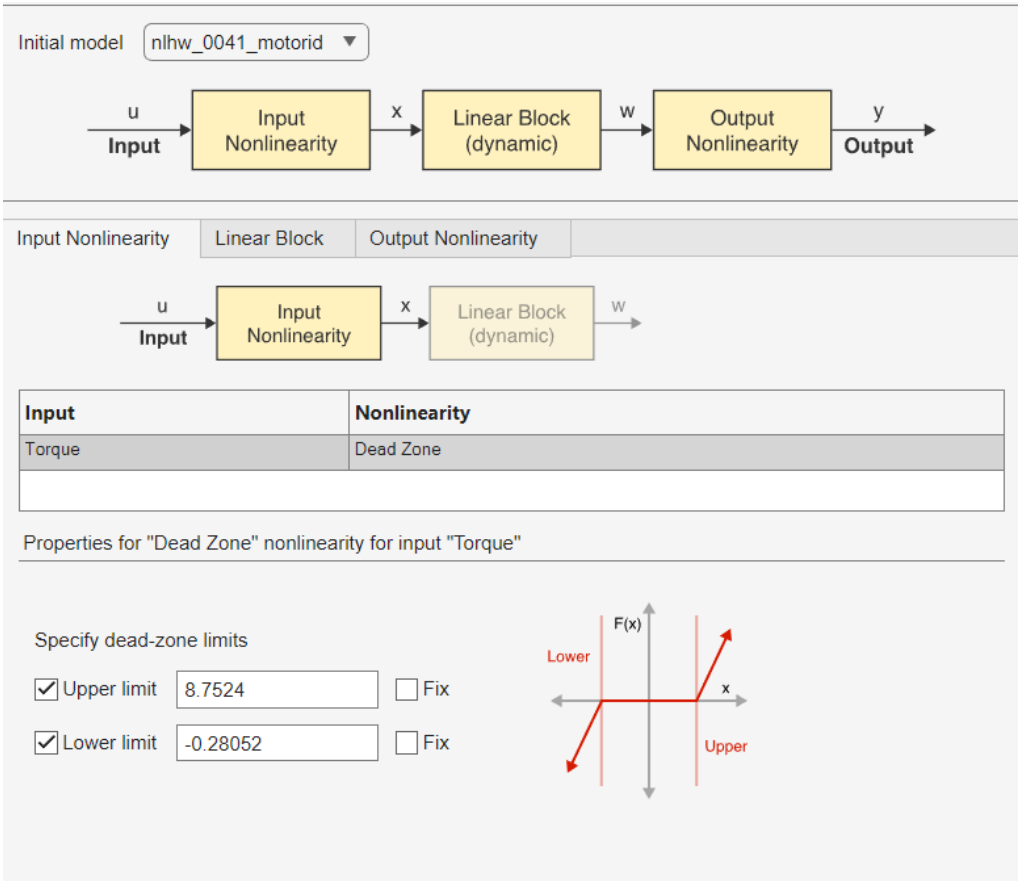

Figure 5.5: nonlinearity input HW model

A non-linear dead zone was considered for a non-linear characteristic. The reference function in is *idDeadZone* is an object that stores the nonlinearity estimator of the dead zone for Hammerstein-Wiener model estimation.

It is used to define a nonlinear function $y=F(x,\theta)$, where y and x are scalars and θ represents the parameters a and b, which define the zero interval.

The dead-zone nonlinearity function has the following characteristics:

$$\begin{aligned} a \le x < b \quad & F(x) = 0 \\ x < a \quad & F(x) = x - a \\ x \ge b \quad & F(x) = x - b \end{aligned}$$

In this case the parameters are:

a = - 0.28052 as lower limit

b = 8.7524 as upper limit

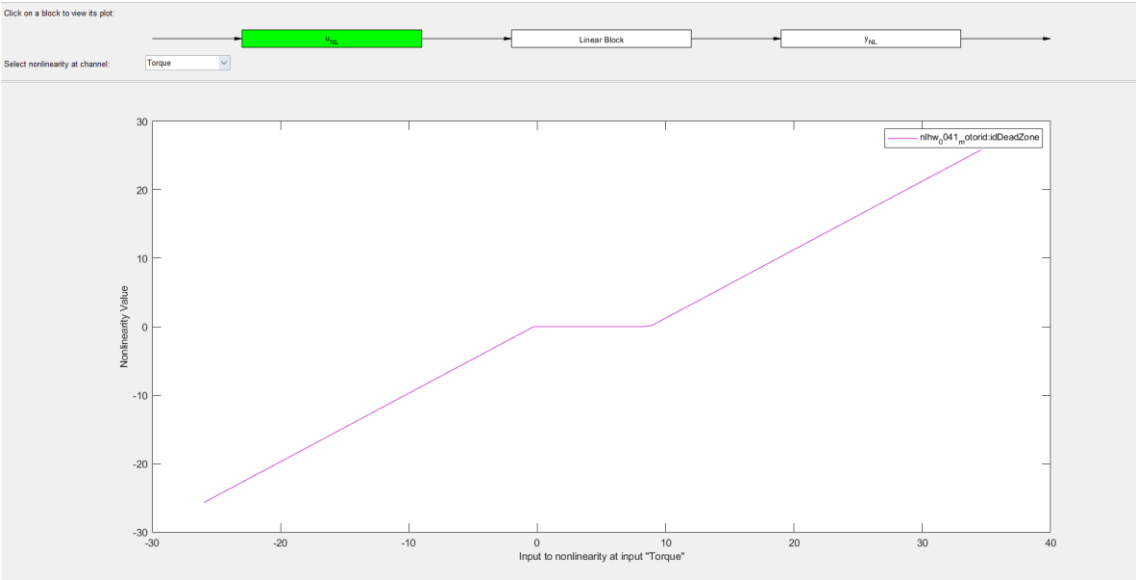

Figure 5.6: nonlinear input dead zone

The bode diagram analysis shows that in the first part, at low frequencies, the behaviour remains constant. At intermediate and high frequencies there is attenuation attributable to, in the case under consideration, mechanical elements such as gearboxes and dampers such as the elastic coupling.

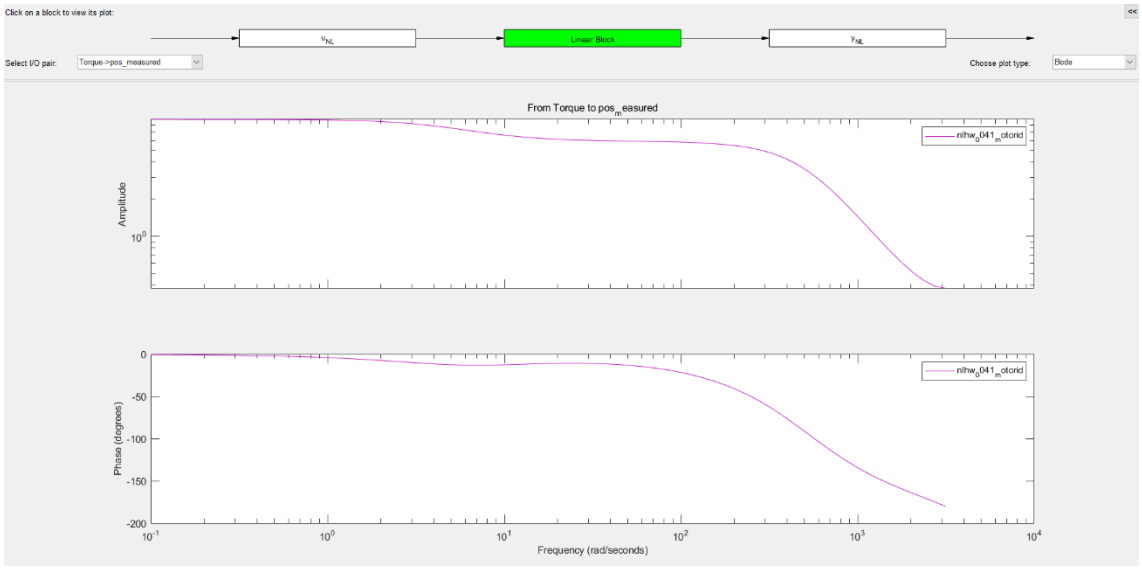

Figure 5.7: frequency response linear model HW

In this linearisation method, there is an alternation of non-linear and linear blocks. The last block present, the output is the measured position whose non-linearity was evaluated using the piecewise linear function indicating 10 breakpoints whose location is indicated in the following vector:

Breakpoint:

[-92.3854616535816 1.20601779461058 131.524758378186 277.324459261305 421.935107091707 566.545442669064 711.155778812021 855.766114522873 1000.37645023732 1144.98678595497].

The nonlinear point referred to the breakpoints are:

Nonlinearity value: [-0.1677709410 -0.165078178614813 -0.155607707750008 -0.164796537730145 -0.176534186550449 -0.185671143317075 -0.187636356671893 -0.189836846097723 -0.186725616831728 -0.174846085728571].

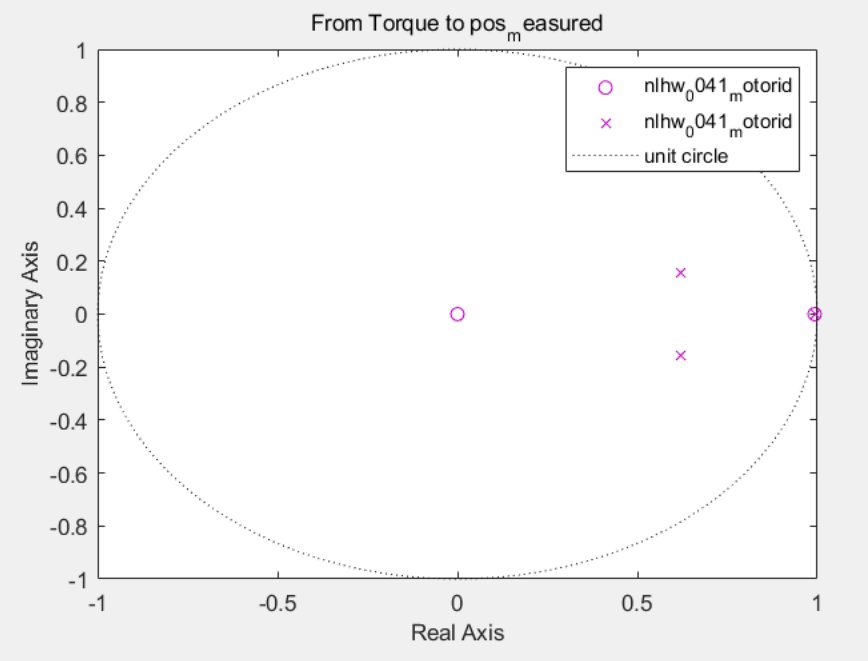

Figure 5.8: poles and zero position linear model

An analysis of the positioning of the poles and zeros referred to the linear block shows how the position of poles close to the real axis suggests overdamping behaviour, while those closer to the circumference have an effect on the system's response. The zero near the origin indicates that there is a component present that affects the system response with a slow response. At high frequencies as in the present case, there is an attenuation of the oscillation. This is reflected by the components present in the system and their purpose.

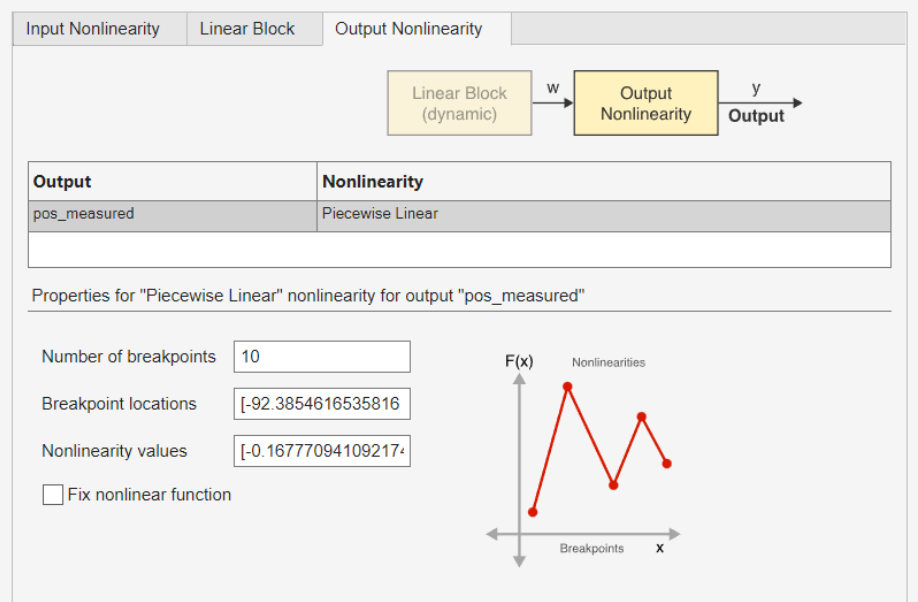

Figure 5.9: nonlinear output HW

The piecewise-linear function refers to the MATLAB command *idPiecewiseLinear* is an object that stores the piecewise-linear nonlinearity estimator. This command is used to define a nonlinear function of the following type $y=F(x, \theta)$ where y and x are scalar elements and θ represents the number of breakpoints and the nonlinearity value referred to at the breakpoint. The function F is a non-linear function at breakpoints. There are n breakpoints (x_k, y_k) with $k=1...n$ such that $y_k = F(x_k)$.

The F function is linearly interpolated between the breakpoints. The F-function is also linear to the left and right of the extreme breakpoints. The slope of these extensions is a function of the breakpoints xi and yi. The breakpoints are ordered by ascending values of x, which is important when setting a specific breakpoint to a different value. There is a small difference between the values of the set breakpoints and those stored in the object, because the toolbox has a different internal representation of the breakpoints.

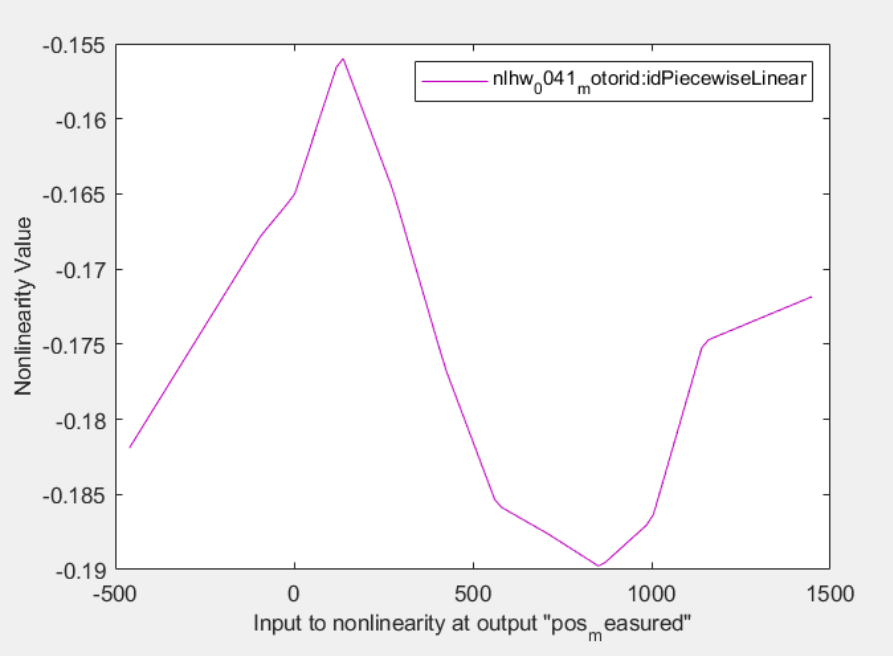

Figure 5.10: nonlinear output piecewise

The generated model has a fitting of 91.28%. The performance with respect to the output is roughly comparable unless there is some loss of performance during the peaks of the waveforms. The comparison was made against a data set referring to the signal with white noise added to the current loop.

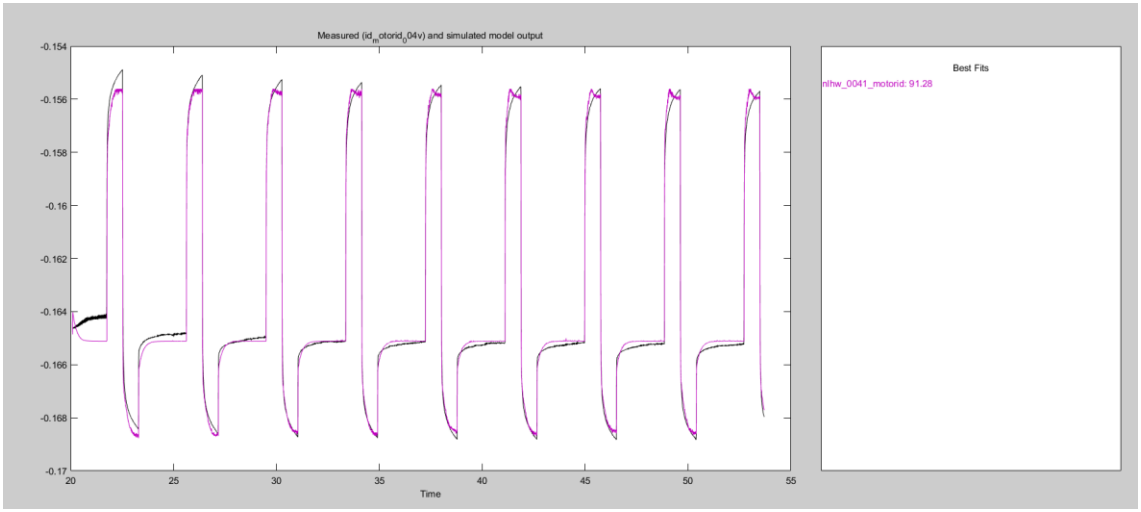

Figure 5.11: validation model motor adaptor identification

5.4 Ball screw – cutting head identification

The part of the system consisting of the ball screw lead and the cutting head is included between the signals from the encoder, measured position, and the interferometric laser, laser_position.

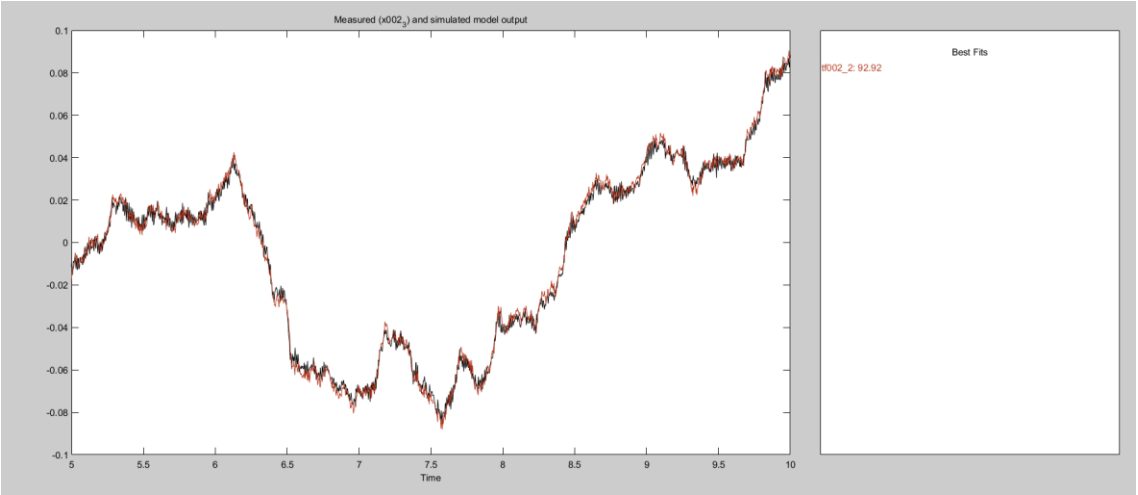

Figure 5.12: validation BS identification model -1st dataset

The identification was done starting with the 2nd test in which white noise was added to the velocity loop. The fitting achieved with respect to a new set of data, in the case in figure with respect to the third movement performed in the 2nd test, reach values above 90%. When compared to other tests also performed, the values achieved are acceptable in terms of fitting and also with respect to the MSE (mean square error), the value of which in the case in the figure is 7.095e-5.

For comparison, the prediction output compared to the first test in which the system was not excited by the addition of white noise is also included.

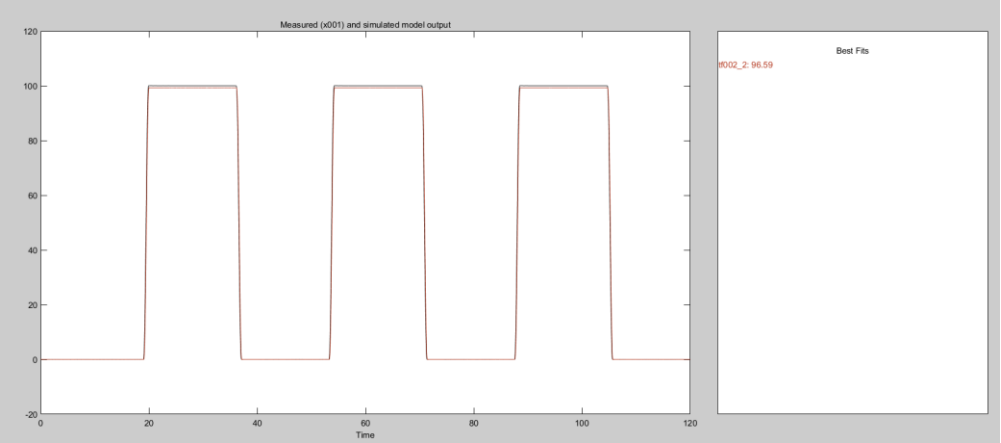

Figure 5.13: validation BS identification models- 2nd dataset

The fitting achieved is 96.59%. It is interesting to note that the choice of the data range referred to a specific test provides a good identification even with respect to tests with different frequencies. As a verification, an identification was performed starting with data from test 1 and the same model was validated on a dataset from the same test and compared against the model mentioned above.

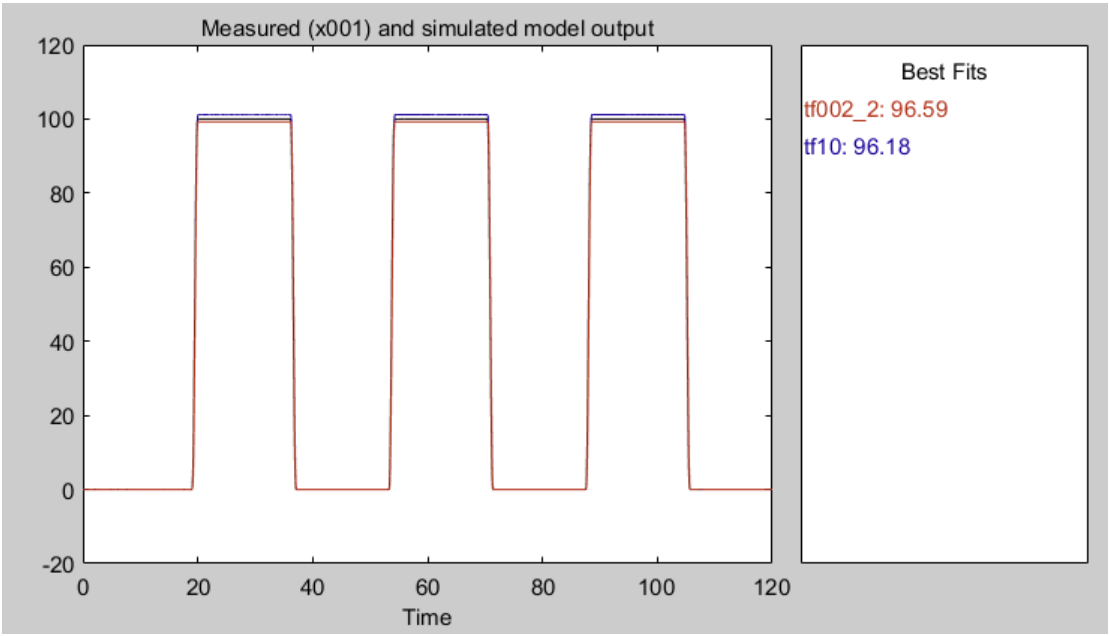

Figure 5.14: Comparison with different tf during validation ID model

The result obtained shows that the brown curve (tf002) referring to the data from the system excitation has a higher fitting value than the blue model (tf10) obtained from the first test.

The iterative process of finding the best transfer function shows that increasing the number of poles and zeros does not lead to an increase in fitting. The transfer function is as follows:

```
From input "pos_measured" to output "pos_laser":
   3346 s + 7.554e04
-----------------------
s^2 + 3024 s + 7.535e04
```

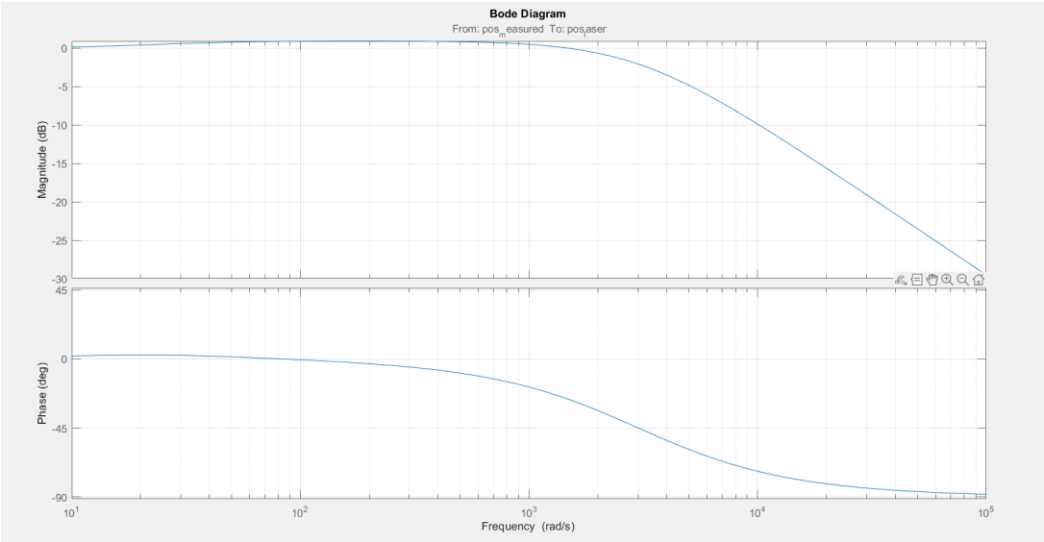

Figure 5.15: Frequency response from BS's tf

The system consists of zero and two poles. At high frequencies, there is a slope of -20db/dec due to the presence of the pole. By analysing the transfer function, the response is not position-dependent but speed-dependent. The two poles at the denominator highlight the mechanical elements present in this system, namely stiffness and damping.

$$p_1 = -2998\frac{rad}{s}$$

$$p_2 = -25{,}1\frac{rad}{s}$$

$$z_1 = -22{,}58\frac{rad}{s}$$

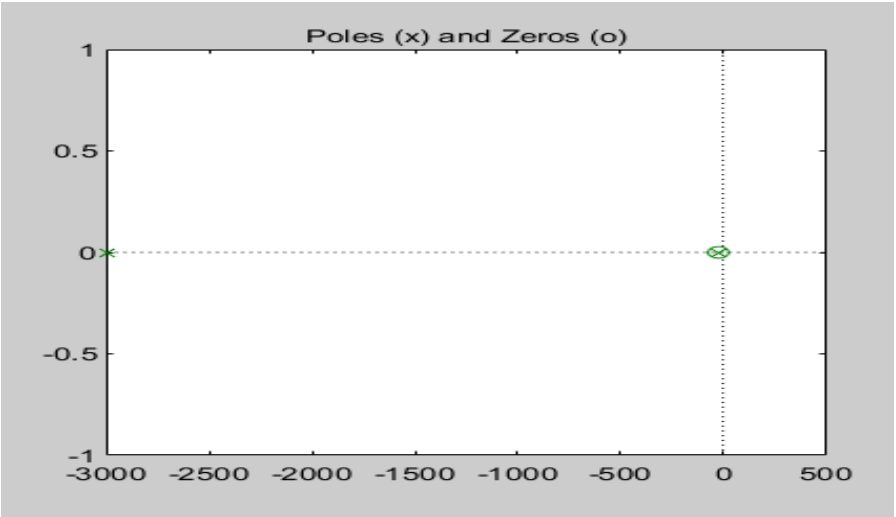

Figure 5.16: poles and zeros position

The two poles have negative real parts bringing the answers to zero so we can speak of stability. Poles are denoted by X and zero by O.

6 First principles modelling: bond graph

The need to be able to change components and verify how the system changes and reacts to new stimuli led to the modelling of a model from physics. The first principles approach used was via the Bond Graph, which relates multi-domain elements by considering the energy exchange that takes place between the components.

The elements related to the bond graph were taken from Chapter 2. In this chapter of the paper, we report the models obtained through this approach

Modelling followed the same approach used for data - driven, i.e. using the intermediate signals acquired during machine tests in order to compare and validate the models used. Finally, an aggregate model was generated for inclusion in the Simulink representation.

6.1 Motor – adaptor modelling

The bond graph modelling of the motor and adaptor was performed in MATLAB for the state-space calculations. The component data are listed in the table below. As can be seen, the motor's electrical domain data are also present in accordance with multi-domain modelling using the bond graph.

Motor	Component	Value	udm	description
	kmot	3900	Nm/rad	motor stifness
	Jmot	4,40E-05	kg m^2	motor inertia
	Ra	6,29	ohm	resistance
	La	5,00E-03	H	inductance
	Kt	0,62	N/A	constat torque
Adaptor	tau	3		gear ratio
	krot	1,10E+04	Nm/rad	stiffness spring

Table 6-1: datasheet about motor adaptor for BG modelling

Once the data was defined, the model was generated according to the guidelines mentioned in the last chapter. Through the inclusion of casualties, the constraints and states of the system were defined, from which the calculation was developed to obtain the equations of state and state space.

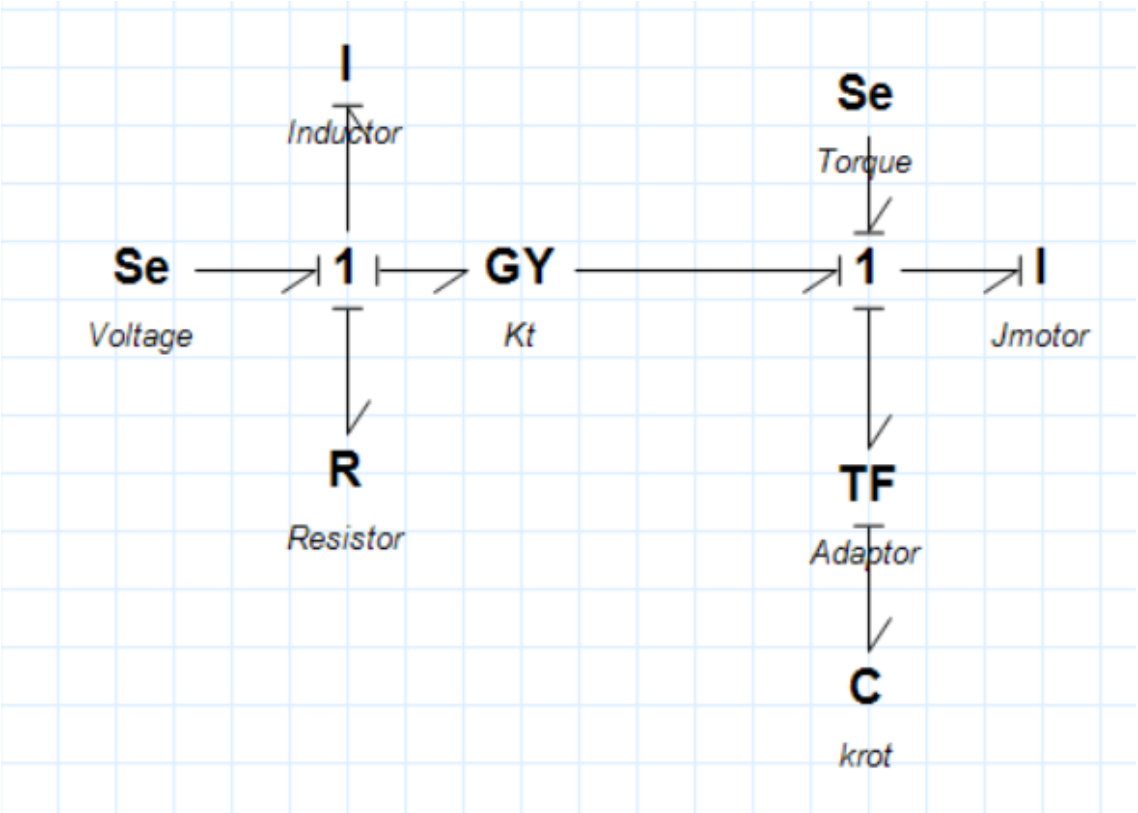

Figure 6.1: Motor adaptor BG

The system has two sources. The voltage is from the drive, which processes the position signal from the CN as seen. The other source present takes into account external electrical torques such as the motor's resistor torque and any friction. This was the starting point for defining the system's constraints and casualties. There are three system states, related to the inductor, the motor inertia and the torsional joint stiffness.

Se : V	$e_1 = T$	
I : L	$\mathbf{e_2 = p_2}$	$p_2 = L\, f_2$
R:R	$e_3 = R\, f_3$	
GY : Kt	$e_5 = Kt\, f_4$	
	$e_4 = Kt\, f_5$	
Se : Cr	$e_6 = Cr$	
I : Jmot	$\mathbf{e_7 = p_7}$	$p_7 = Jmot\, e_9$
TF :τ	$f_9 = \tau\, f_8$	
	$e_8 = \tau\, e_9$	
C : Krot	$\mathbf{f_9 = q_9}$	$e_9 = Krot\, q_9$

The table summarizes the relationships and the link between flow and effort of the respective components. Starting from these relationships and the casualty relative to junctions 1 and 0, the following relationships are obtained:

$$\dot{p_2} = V - \frac{R}{L}\dot{p_2} - \frac{K_t}{J_{mot}} p_7$$

$$\dot{p_7} = \frac{K_t}{L} p_2 - \dot{C_r} - \tau\, K_{rot} q_9$$

$$\dot{q_9} = \frac{\dot{\tau}}{J_{mot}}\, p_7$$

From these equations, one can derive the state space by defining the output, which in the present case corresponds to the motor speed and torque input to the ball screw represented by the following equations:

$$motor_{speed} = \frac{p_7}{Jmot}$$

$$BS_{speed} = \frac{\tau}{J_{mot}}\, q_9$$

The motor equation was subsequently integrated to evaluate the motor position and compare it with what was obtained from the comparison model. From the equations, the matrices A, B, C, D for the state space is defined.

$$\dot{x} = \begin{pmatrix} \dot{p_2} \\ \dot{p_7} \\ \dot{q_9} \end{pmatrix} = \begin{pmatrix} -\frac{R}{L} & -\frac{K_t}{J_{mot}} & 0 \\ \frac{K_t}{L} & 0 & -\tau\, K_{rot} \\ 0 & \frac{\tau}{J_{mot}} & 0 \end{pmatrix} \begin{pmatrix} p_2 \\ p_7 \\ q_9 \end{pmatrix} + \begin{pmatrix} 1 & 0 \\ 0 & 1 \\ 0 & 0 \end{pmatrix} \begin{pmatrix} V & C_r \end{pmatrix}$$

$$y = \begin{pmatrix} 0 & \frac{1}{J_{mot}} & 0 \\ 0 & \frac{\tau}{J_{mot}} & 0 \end{pmatrix} \begin{pmatrix} f_8 \\ q_9 \end{pmatrix} + 0$$

The state space is created in MATLAB to obtain a Simulink block via the ss function.

6.2 Ball screw – cutting head modelling

The second modelling concerns the ball screw lead system and the cutting head. As with the identification from data, the same data was used here. The

generated model has fewer elements than the previous one and the input signal used is a source flow, i.e. the encoder position, and the position at the output of the head was evaluated as output after appropriate integration.

p	13,33	mm	screw ball ratio
kv	3,80E+08	N/m	BS stiffness
mv	6,13E-01	kg	screw mass
m_{head}	25	kg	cutting head mass

Table 6-2: datasheet about BS - cutting head

The bond graph about the system below:

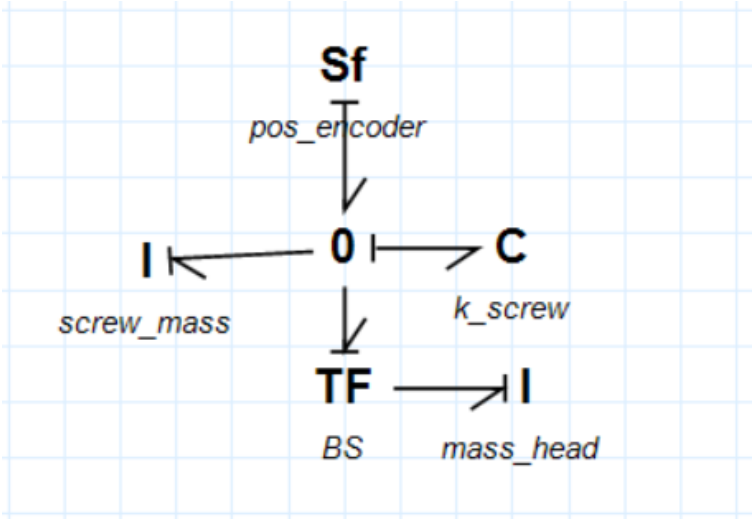

Figure 6.2: BG modelling about BS and cutting head

From the graph, in this case there is only one input, and the casualty analysis yields three states related to screw mass, screw stiffness and mass of the cutting head, respectively.

Sf : $pos_{encoder}$	$f_1 = pos_{encoder}$	
I : m_v	$\mathbf{e_2 = p_2}$	$p_2 = m_v f_2$
C : k_v	$\mathbf{f_3 = q_3}$	$e_3 = k_v q_3$
TF : p	$e_5 = e_4 / p$	
	$f_4 = f_5 / p$	
I : m_t	$\mathbf{e_5 = p_5}$	$p_5 = m_t f_5$

From the relations above and the analysis of causality, we obtain the equations of the system

$$\dot{p_2} = k_v \, q_3$$

$$\dot{q_3} = pos_{enc} - \frac{p_2}{m_v} - \frac{1}{p}\frac{p_5}{m_t}$$

$$\dot{p_5} = \frac{k_v}{p} \, q_3$$

The output is:

$$beam_{speed} = \frac{p_5}{m_t}$$

Here too, the velocity will be integrated to obtain the position of the beam and compare it with the data-driven model.

The state space is as follows:

$$\dot{x} = \begin{pmatrix} \dot{p_2} \\ \dot{p_7} \\ \dot{q_9} \end{pmatrix} = \begin{pmatrix} 0 & k_v & 0 \\ \frac{1}{m_t} & 0 & -\frac{1}{p \, m_t} \\ 0 & \frac{k_v}{p} & 0 \end{pmatrix} \begin{pmatrix} p_2 \\ p_7 \\ q_9 \end{pmatrix} + \begin{pmatrix} 0 \\ 1 \\ 0 \end{pmatrix} (pos_{enc})$$

$$y = \begin{pmatrix} 0 & 0 & \frac{1}{m_t} \end{pmatrix} (f_5) + 0$$

The splitting of the System into two parts was done in order to improve the comparison to the identification made earlier. The model can be made whole by linking both parts as shown below.

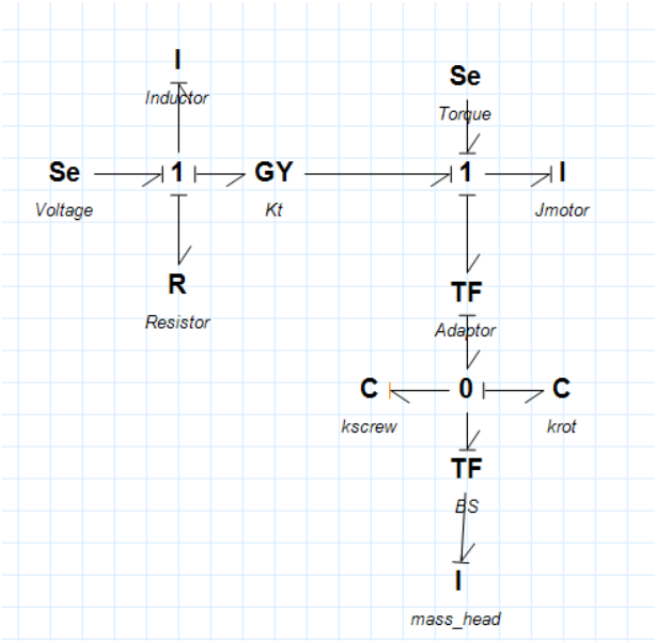

Figure 6.3: overall BG system

The main difference between the models is in the presence of a derivative state placed between the adaptor and the ball screw lead. The decision not to consider the entire model is aimed at assessing the effect of each component by estimating and validating the individual items.

7 ANALYSIS AND COMPARISON OF MODELS

In this chapter of the dissertation, the models generated with the two approaches are compared. To carry out this comparison, it was necessary to use Matlab@Simulink in which the modelled elements were implemented and developed using the toolbox for data-driven identification and using the MATLAB environment for first principles modelling.

The Simulink diagram consists of the block in which the control signals, i.e. position, velocity and acceleration, are generated. Subsequent blocks relate to the part of the drive where the three control loops: position, speed and current. The output signal corresponds to the input voltage signal in the modelled part.

The last blocks represent the model validation blocks where the tests and comparisons relating to the Z - axis were carried out.

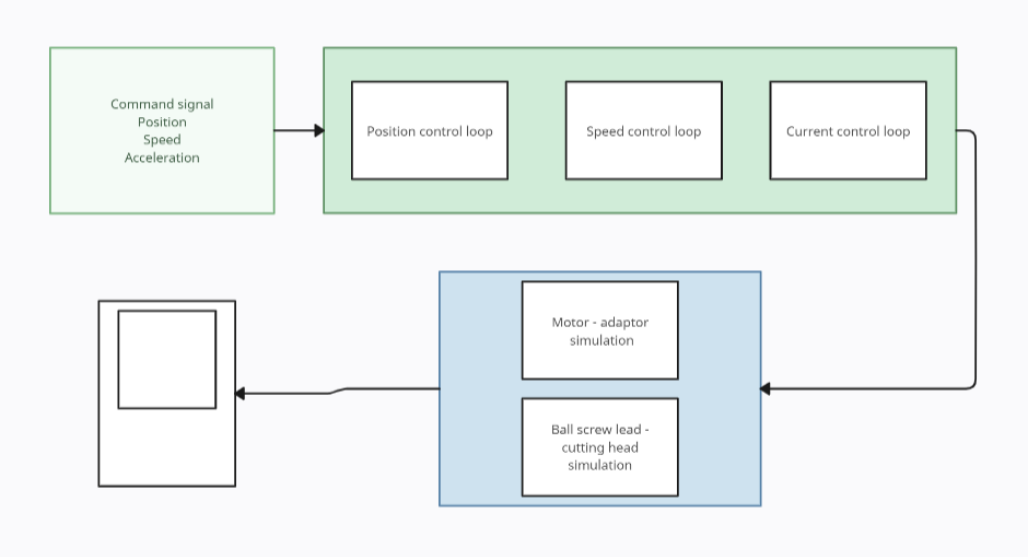

Figure 7.1: block scheme for comparison models

The first comparison made was between motor - adaptor models. The input signal used is torque. As seen in the previous chapter, the output of these models considers the position of the ball screw. It is logical to expect a non-optimal trend in the output signal as the parameters constituting the second evaluated system present in the exchange interface are not considered in this model. The aim is to assess how the systems respond to the stimuli and whether the first principles model provides information on the components present.

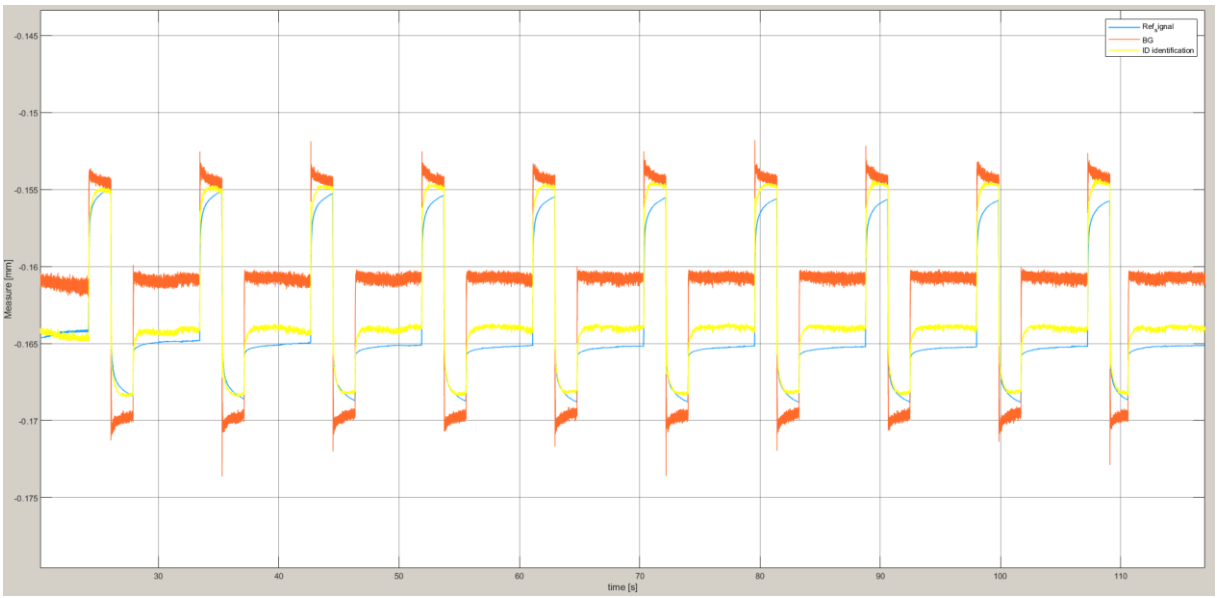

Figure 7.2: comparison output signal models respect reference signals- 1st modelling

The three signals being compared are shown in the figure. In blue is the reference signal, in this case the encoder position. In yellow is the signal generated by the Hammerstein model, and in red the model obtained via the BG approach.

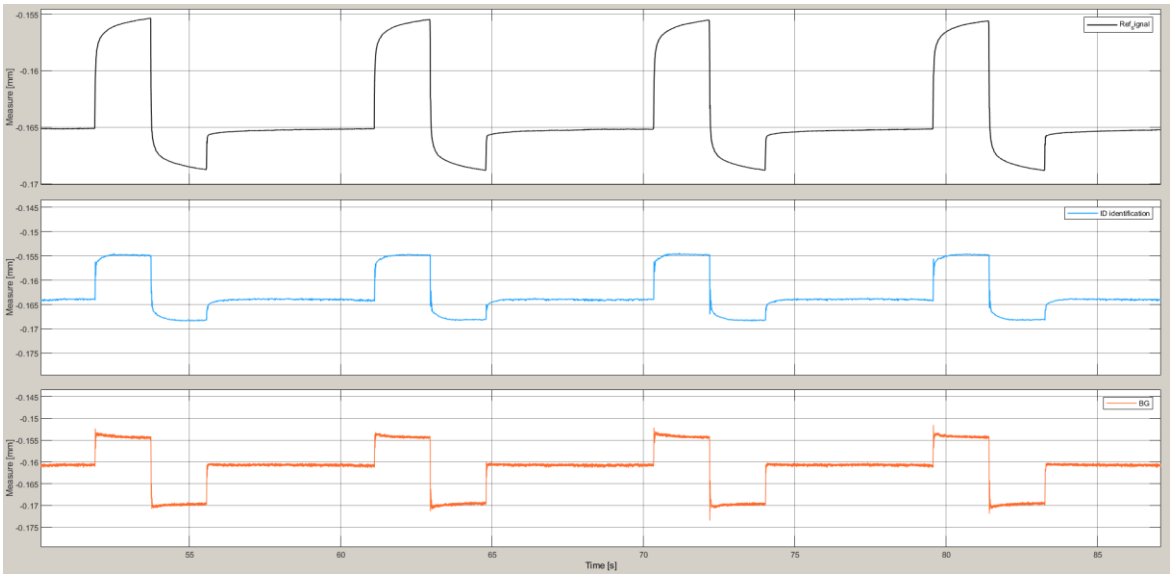

Figure 7.3: separate output signal – 1st modelling

By zooming in on a few wave fronts, it can be observed that the trend and order of magnitude of the three curves is similar. However, the output obtained from the model generated through data-driven identification manages to follow the output signal better. The first principles model results as a trend in line with the two above, but in the rapid change of trajectory it lags, amplifying the signal. It is interesting to note how in the rise or fall the curves overlap, emphasizing how the problem of the model created is contained in the response to steady states with a damping element bound.

In the second model comparison, an output signal from the cutting head is compared. The system as seen consists of a ball screw lead that transforms the motion in which damping elements and stiffnesses were also considered during BG modelling. In the graph, the curves are overlapped to the nearest µm.

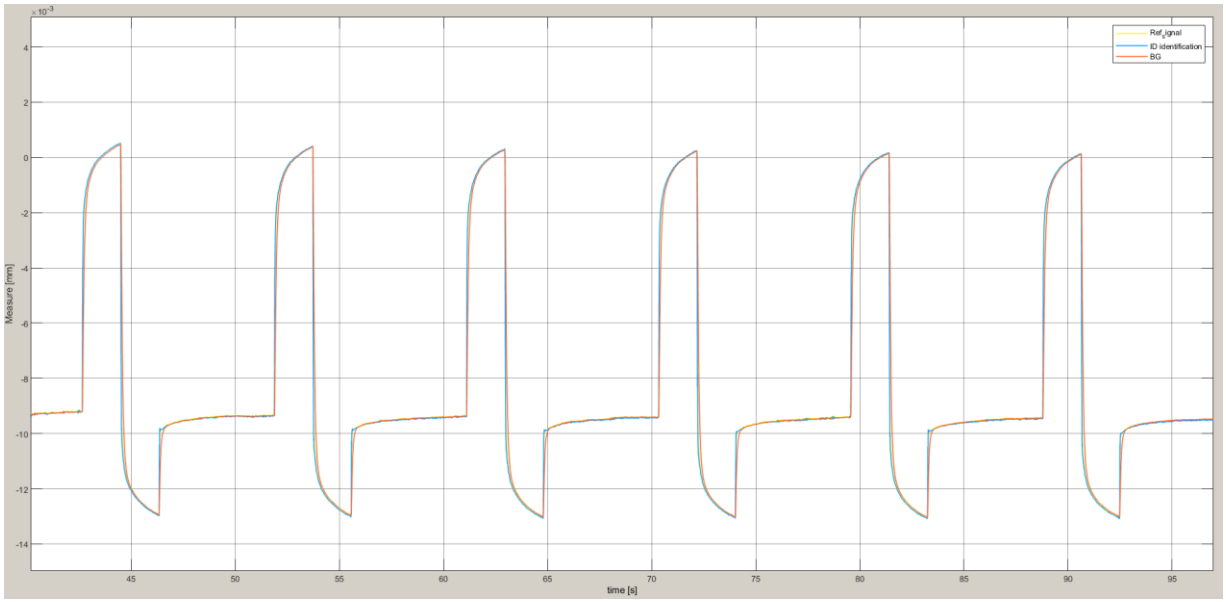

Figure 7.4: comparison output signal models respect reference signals – 2nd modelling

After zooming in, it can be noticed that the two model-related trends are similar. Compared to the previous case, the trend of the model identified via the data is confirmed, which follows the trend of the reference signal. The model generated by means of the BG also follows the trend of the signal whose only loss of alignment occurs in the low amplitude rising edge where the signal is slightly smooth but still negligible.

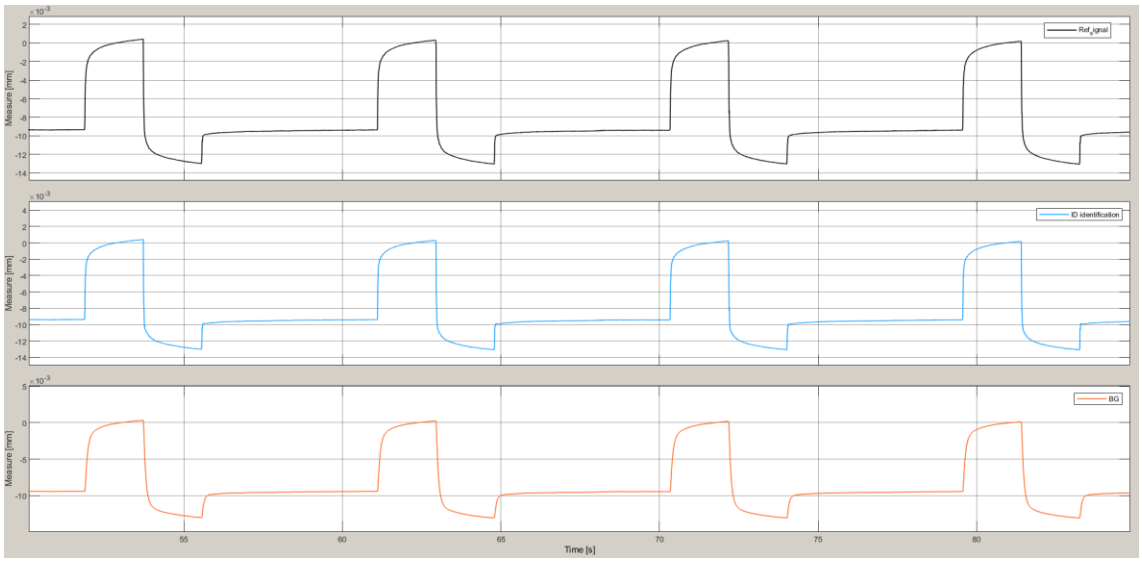

Figure 7.5: separate output signal – 2nd modelling

After validation and comparison of the model, a test was performed by changing the data of a component in the system. Specifically, the mass of the cutting head was changed to test how the system reacted to an increase in mass with the same input signal. The result of the test is shown in the figure below.

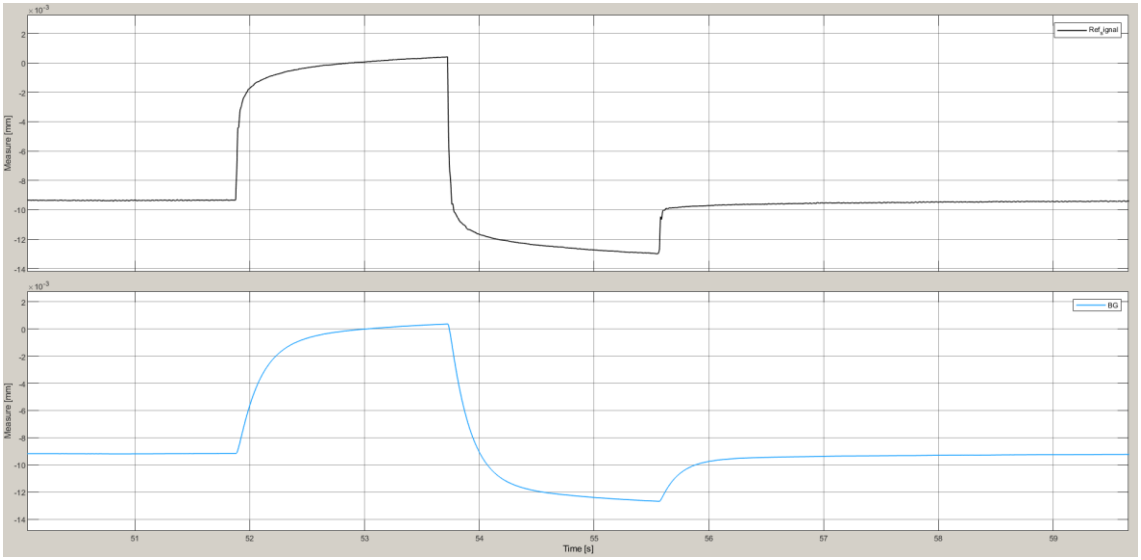

Figure 7.6: test with head mass changes respect previus singnal

In the figure, it can be seen that with an increase in mass and the same input, there is a less rapid upward and downward trend as is the case with data from the datasheet. This trend is in agreement with what can be expected from physics. In order for this signal not to lose performance, it is necessary to check the input, which in the case under consideration is related to the current and torque supplied to the motor.

8 Conclusion

In the conducted study, the identification and modelling of a system composed of an electromechanical axis were addressed. The activity was carried out, after a preliminary phase of system contextualization, with tests performed on the machine, acquiring movements of the cutting head through an interferometric laser.

The data-driven identification was performed using the SystemIdentification@Matlab toolbox. The creation of a model using a first principles approach was carried out through the Bond Graph approach. The second modelling approach was conducted to have a custom model to verify how the system reacts to the change or replacement of elements.

Four different tests were performed on the machine to first identify the dynamics of the Z-axis. The four tests had different characteristics, particularly three of which involved adding white noise at various points of the drive, specifically (velocity, torque, and current).

The test with white noise added to the velocity control loop aimed to best identify the mechanical parameters. The data obtained from this test led to the identification of the mechanical part related to the ball screw lead.

The third test involved adding white noise to the torque, thus bypassing the control action. The signal was very noisy, resulting in no interesting data for identification purposes.

The fourth test was used to identify and validate the part related to the motor adaptor. The test involved adding white noise to the current control loop. Subsequently, a data set was used for validation and for comparing the created models.

The first test did not involve any white noise but was conducted by performing movements of the axis generating a square wave. Through this test, a frequency response analysis of the drive was carried out. In fact, the test allowed the acquisition of the input position of the drive and was used as an input signal for identifying the drive, using the torque input to the motor as the output.

The availability of signals at different points in the system allowed for identification and subsequent modelling to be done in parts.

The motor, adapter, and torsional stiffness composed one part of the system, while the cutting head and the ball screw lead formed the second part.

The first part of the system was identified using a nonlinear method, the Hammerstein-Wiener Models, considering torque as the nonlinear input and encoder position as the nonlinear output.

The second part was included between two position signals and was identified and represented using a transfer function.

A part-wise procedure was also carried out for modelling using the bond graph approach. The models generated with this type of approach follow the reference signals. The model of the motor adapter has a behaviour that represents the desired output but with a delayed response to small variations, likely due to insufficiently identified damping effects.

On the other hand, in the head–ball screw system, the model's response allowed an evaluation even when changing the value of the cutting head mass.

For the short-term purposes of the company, the data-driven model is sufficient for evaluations regarding the tracking algorithm in which the signals used are like the signals used for validation.

For future purposes, the physical model can be improved by ad-hoc tests to identify damping and friction elements.

BIBLIOGRAFY

[1] K. Kyriakopoulos and G. Saridis, *Minimum jerk path generation*, vol. 1. 1988, p. 369 vol.1.

[2] L. Lennart, 'System Identification Toolbox User's Guide'.

[3] PrimaPower - Prima Idustrie group, 'Laser Genius+ | Prima Power'. [Online]. Available: www.primapower.com/it/tecnologie/taglio-laser-2d/macchine-il-taglio-laser-2d/laser-genius-plus

[4] Rexroth - Bosch company, 'IndraDrive MPx-16 to MPx-21 and PSB Parameters'. [Online]. Available: www.boschrexroth.com/it/it/search.html?q=R911328651

[5] P. Czop, G. Kost, D. Sławik, and G. Wszołek, 'Formulation and identification of First- Principle Data-Driven models', *Journal of Achievements in Materials and Manufacturing Engineering*, vol. 44, no. 2, 2011.

[6] J. Swevers, W. Verdonck, and J. De Schutter, 'Dynamic Model Identification for Industrial Robots', *IEEE Control Systems Magazine*, vol. 27, no. 5, pp. 58–71, Oct. 2007, doi: 10.1109/MCS.2007.904659.

[7] Matworks, 'Black-Box Modeling - MATLAB & Simulink'. [Online]. Available: https://www.mathworks.com/help/ident/ug/black-box-modeling.html

[8] M. Krell and S. Hergert, 'The Black Box Approach: Analyzing Modeling Strategies', in *Towards a Competence-Based View on Models and Modeling in Science Education*, A. Upmeier zu Belzen, D. Krüger, and J. van Driel, Eds., Cham: Springer International Publishing, 2019, pp. 147–160.

[9] B. Sohlberg and E. W. Jacobsen, 'Grey box modelling – branches and experiences', *IFAC Proceedings Volumes*, vol. 41, no. 2, pp. 11415–11420, Jan. 2008.

[10] ‘Estimate Linear Grey-Box Models - MATLAB & Simulink - MathWorks Italia’. [Online]. Available: https://it.mathworks.com/help/ident/ug/estimating-linear-grey-box-models.html

[11] Jordi Villar Venini, ‘Model-Based Design per la Modellazione Fisica’, MathWorks, Apr. 2024.

[12] J. Felez, G. Romero, J. Maroto, and M. L. Martinez, ‘Simulation of Multi-body Systems Using Multi-bond Graphs’, in *Bond Graph Modelling of Engineering Systems: Theory, Applications and Software Support*, W. Borutzky, Ed., New York, NY: Springer, 2011, pp. 323–354. [Online]. Available: https://doi.org/10.1007/978-1-4419-9368-7_9

[13] P. P. J. van den Bosch and A. C. van der Klauw, *Modeling, Identification and Simulation of Dynamical Systems*. London: CRC Press, 2020.

[14] G. C. Goodwin and R. L. Payne, *Dynamic System Identification: Experiment Design and Data Analysis*. Academic Press, 1977.

[15] T. Soderstrom, H. Fan, B. Carlsson, and S. Bigi, ‘Least squares parameter estimation of continuous-time ARX models from discrete-time data’, *IEEE Trans. Automat. Contr.*, vol. 42, no. 5, pp. 659–673, May 1997.

[16] R. Diversi, R. Guidorzi, and U. Soverini, ‘Identification of ARX and ARARX Models in the Presence of Input and Output Noises’, *European Journal of Control*, vol. 16, no. 3, pp. 242–255, Jan. 2010.

[17] A. Wills, T. B. Schön, L. Ljung, and B. Ninness, ‘Identification of Hammerstein–Wiener models’, *Automatica*, vol. 49, no. 1, pp. 70–81, Jan. 2013.

[18] V. Z. Marmarelis, ‘Identification of nonlinear systems by use of nonstationary white-noise inputs’, *Applied Mathematical Modelling*, vol. 4, no. 2, pp. 117–124, Apr. 1980.

[19] Er-Wei Bai, ‘An optimal two stage identification algorithm for Hammerstein-Wiener nonlinear systems’, in *Proceedings of the 1998 American Control Conference. ACC (IEEE Cat. No.98CH36207)*, Philadelphia, PA, USA: IEEE, 1998, pp. 2756–2760 vol.5. [Online]. Available: http://ieeexplore.ieee.org/document/688354/

[20] MathWorks Italia, ‘What are Hammerstein-Wiener Models’. [Online]. Available: https://it.mathworks.com/help/ident/ug/what-are-hammerstein-wiener-models.html

[21] A. K. Samantaray and B. O. Bouamama, *Model-based Process Supervision: A Bond Graph Approach*. Springer Science & Business Media, 2008.

[22] Lorcan Stuart Peter Stillwell Smith, ‘Bond graph modelling for physical system’. Faculty of engineering - Glasgow university.

[23] J. F. Broenink, ‘Bond Graphs: A Unifying Framework for Modelling of Physical Systems’, in *Foundations of Multi-Paradigm Modelling for Cyber-Physical Systems*, P. Carreira, V. Amaral, and H. Vangheluwe, Eds., Cham: Springer International Publishing, 2020, pp. 15–44. [Online]. Available: https://doi.org/10.1007/978-3-030-43946-0_2

[24] Wittestain, ‘Alpha advance line’. [Online]. Available: alpha.wittenstein.it/prodotti/alpha-advanced-line/

[25] Rexroth - Bosch company, ‘Azionamenti a vite’. [Online]. Available: www.boschrexroth.com/it/it/search.html?q=R999001187

[26] *Identification of Linear Systems*. 2014. Accessed: Jul. 12, 2024. [Online]. Available: https://shop.elsevier.com/books/identification-of-linear-systems/schoukens/978-0-08-040734-0